Available online at www.sciencedirect.com

ScienceDirect

journal homepage: www.elsevier.com/locate/he

Assessment of integration of methane-reduced ceria chemical looping CO_2/H_2O splitting cycle to an oxy-fired power plant

Azharuddin Farooqui [a,b,c,*], *Archishman Bose* [d], *Marta Boaro* [e], *Jordi Llorca* [c], *Massimo Santarelli* [a,f]

[a] *Department of Energy, Politecnico di Torino, Italy*
[b] *German Aerospace Center (DLR), Institute of Engineering Thermodynamics, 70569, Stuttgart, Germany*
[c] *Institute of Energy Technologies, Department of Chemical Engineering and Barcelona Research Center in Multiscale Science and Engineering, Universitat Politècnica de Catalunya, Barcelona, Spain*
[d] *Marine and Renewable Energy Research (MaREI) Centre, Environmental Research Institute, School of Engineering and Food Science, University College Cork, Lee Road, Cork, T23 XE10, Ireland*
[e] *Polytechnic Department of Engineering and Architecture (DPIA), Universita di Udine, Italy*
[f] *Department of Mechanical and Industrial Engineering, University of Illinois at Chicago, Chicago, IL, United States*

HIGHLIGHTS

- Kinetic study of methane-driven CO_2/H_2O (CL) splitting is investigated.
- Redox reaction kinetics found to follow Avrami-Erofe'ev model.
- A moving bed CL unit is integrated to oxy-fired plant for efficiency improvement.
- The CL efficiency found to be 42.8% with system efficiency of 50.9%.

GRAPHICAL ABSTRACT

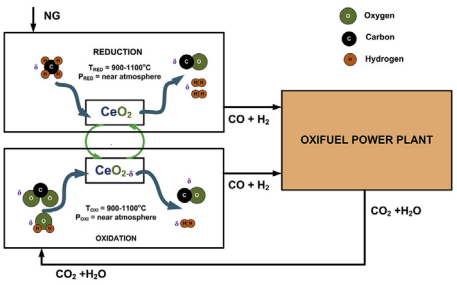

ARTICLE INFO

Article history:
Received 4 October 2019
Received in revised form
19 December 2019
Accepted 26 December 2019
Available online xxx

Keywords:
Chemical looping
CO_2/H_2O splitting
Kinetics

ABSTRACT

In this paper, we investigated the effect of reaction kinetics and moving bed reactors for chemical looping (CO_2/H_2O) splitting unit (CL) that produces syngas and fed back to the power plant to gain the efficiency loss due to carbon capture. The reduction reactor (RED) produces methane is partially oxidized to make syngas and reducing the non-stoichiometric ceria which is transported to oxidation reactor (OXI) where the flue gases (CO_2 and H_2O) split to produce syngas. We developed the kinetics for methane reduced ceria and CO_2/H_2O splitting in a tubular reactor for an operating temperature range of (900 −1100 °C) for different methane concentration which yielded to Avrami-Erofeev (AE3) model fits well for both redox reaction with different reaction constants. A moving bed reactors system is developed representing RED and OXI reactors of CL unit with kinetics hooked to the model in Aspen Plus with FORTRAN code. The effect of thermodynamics and

* *Corresponding author*. Department of Energy, Politecnico di Torino, Italy.
E-mail addresses: azharuddin.xxx@polito.it, azharuddin0613@gmail.com (A. Farooqui).
https://doi.org/10.1016/j.ijhydene.2019.12.182

Please cite this article as: Farooqui A et al., Assessment of integration of methane-reduced ceria chemical looping CO_2/H_2O splitting cycle to an oxy-fired power plant, International Journal of Hydrogen Energy, https://doi.org/10.1016/j.ijhydene.2019.12.182

Experimental
System analysis
Moving bed reactors

the kinetics of redox reaction was investigated in the proposed integrated plant. The CL unit efficiency obtained is 42.8% for kinetic-based CL unit compares to 64% for thermodynamic based CL unit. However, the maximum available efficiency of the proposed layout lowered as 50.9% for kinetic-based CL unit plant compare to than 61.5% for thermodynamic based CL unit. However, the proposed plant shows an improvement in the energy efficiency penalty from 11.3% to 3.8% after CCS.

Introduction

Of the different strategies to eradicate the rise of anthropogenic carbon dioxide, carbon capture and sequestration (CCS) is one of the most discussed and investigated by the scientific community. Most often, CCS involves retrofitting the existing heavily invested fossil fuel-based power plants with post-combustion, pre-combustion or oxy-combustion technologies for capture and storage of CO_2. Nonetheless, commercial applications of such technologies still suffer considerably from both economic viability and operational safety, especially while considering the long term storage of CO_2 [1]. As an alternative, CO_2, after conversion to CO, can be used as a versatile chemical for producing either additional electricity [2] or chemicals such as dimethyl ether [3], methanol and other liquid fuels [4].

Several technologies have been investigated for the conversion of CO_2 to CO, including direct dissociation at over 2500 °C. Of these, in the present decade, significant research has been focussed on chemical looping technology using redox metal oxides with high oxygen carrying capacities [5,6]. In a two-step cycle, a suitable metal oxide, also called oxygen carrier (OC) is first reduced either by thermal reduction (Fig. 1(a)) or by reduction with methane (Fig. 1(b)). This results in a loss of oxygen from the metal lattice, forming a metal oxide of lower valence [5,7,8]. Subsequently, the reduced metal oxide could be oxidized back to its higher valence state either with water or CO_2 or a mixture of both to generate high purity H_2 or CO or a mixture of H_2 and CO [5,7–10]. This possibility of efficient utilisation of concentrated solar energy for low cost renewable hydrogen production have driven research towards not only investigating in suitable oxygen carriers, but also on different reduction pathways and system configurations [11,12].

Studies on numerous materials have identified potential candidates for being an effective oxygen carrier in the redox chemical looping cycle. Of them, Fe_2O_3, and CeO_2 are the most attractive at present [13]. In contrast to iron oxide, ceria exhibits a high optical and electrochemical property alongside a large oxygen carrying capacity. Furthermore its fast response to varying temperature and oxygen chemical demand towards the release and acceptance of oxygen in its crystal lattice makes it an attractive oxygen carrier for chemical looping redox cycle [14]. Additionally, its ability to undergo non-stoichiometric reaction without changing its microstructure at higher temperatures is of great benefit to continuous operation of the chemical looping cycle [15]. Although doped

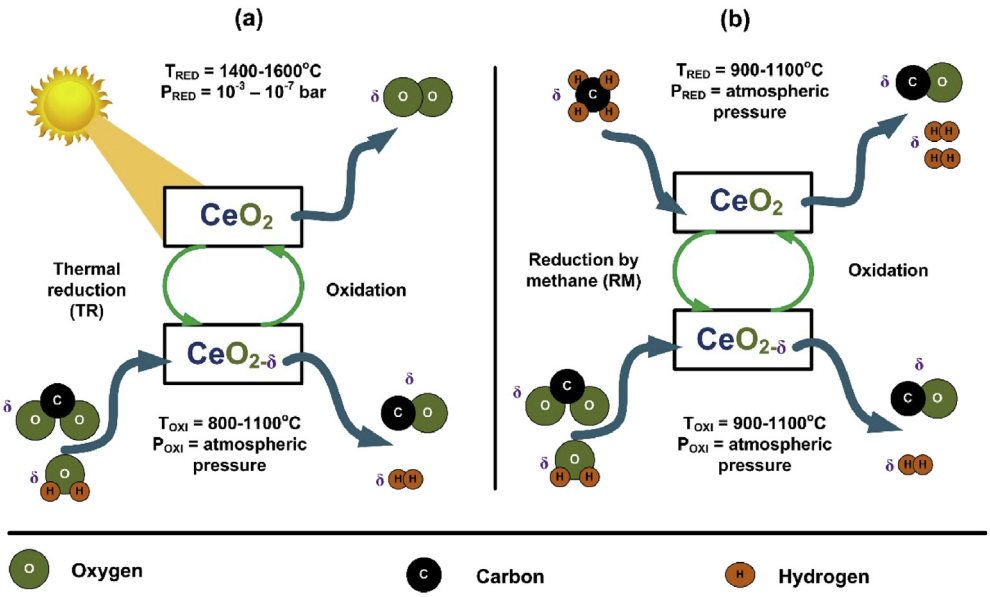

Fig. 1 – A schematic representation of (a) solar thermochemical redox cycle (b) methane-driven chemical looping CO_2/H_2O splitting.

Please cite this article as: Farooqui A et al., Assessment of integration of methane-reduced ceria chemical looping CO_2/H_2O splitting cycle to an oxy-fired power plant, International Journal of Hydrogen Energy, https://doi.org/10.1016/j.ijhydene.2019.12.182

ceria and perovskites are currently being investigated for their high oxygen storage capacity at a relatively lower temperature [6,12,16,17], un-doped ceria would continue to benefit from low cost and ready availability.

Commercial ceria, although is an attractive oxygen carrier for chemical looping, considerable thermal reduction could be achieved only at very high temperatures and extremely low partial pressures [18,19]. Experiments reveal, un-doped Ceria could be reduced by only about 40% of its total theoretical potential at a temperature of 1600 °C and partial pressure of 10^{-7} bar [20]. On the contrary, the exothermic oxidation reaction occurs at relatively low temperatures between 800 and 1100 °C and at atmospheric pressure requiring a temperature and pressure swing between the two redox-steps. The thermal reduction and H_2O and CO_2 dissociation reactions of ceria are summarised in the following Equations (1) and (2).

$$\text{Thermal reduction: } CeO_2 \rightarrow CeO_{2-\delta} + 0.5\delta O_2(g) \quad (1)$$

$$\text{Oxidation: } CeO_{2-\delta} + \delta CO_2(g) \rightarrow CeO_2 + \delta CO(g) \quad (2a)$$

$$\text{Oxidation: } CeO_{2-\delta} + \delta H_2O(g) \rightarrow CeO_2 + \delta H_2(g) \quad (2b)$$

Such challenging operation conditions therefore present significant technological barriers for commercial application of the chemical looping splitting cycle. Especially, attaining such low partial pressures during reduction reaction inherently imposes a high energy penalty. Moreover, the large temperature swing between reduction and oxidation reactions would create an inherent thermodynamic limitation. These challenges of large temperature and pressure swing between reduction and oxidation reactions can be overcome by using methane as the reduction agent. Also termed as the reactive-chemical looping redox cycle, the fuel reduction step, mostly occurring at atmospheric pressures would therefore potentially replace the vacuum operated thermal reduction. Thus, the two-step redox cycle could be operated under isothermal and isobaric conditions between the two reactors. In addition, syngas with an H_2/CO ratio of 2 could also be produced from the partial oxidation of methane, as shown in the following Equation (3).

$$\text{Methane driven reduction: } CeO_2 + \delta CH_4(g) \rightarrow CeO_{2-\delta} + 2\delta H_2\,(g) + \delta CO \quad (3)$$

In recent times, the attention to fuel reduction of ceria has increased immensely [5,21–27]. While some studies focussed on the reactor design [26–32], others experimented with different catalyst promoters such as Pt [33], and Rh [34,35] to enhance the reactivity. Nair and Abanades [26] investigated the solar methane reforming and H_2O/CO_2 splitting for ceria and ceria promoted with MgO and Al_2O_3 in a specially designed solar thermogravimetric reactor. The maximum δ achieved was 0.37 for pure ceria and it increased to 0.431 in the presence of MgO. The reported activation energy was 109 kJ/mol and a reaction order of 0.62. Scheffe's group recently [25,36] conducted experiments on solar methane reforming under different temperatures to investigate the extent of reduction and efficiency in a particle-transport reactor and solar cavity based packed bed tubular reactor for ceria reduction. The particle reactor yielded a non-stoichiometry between 0.002 and 0.25 at 1150–1350 °C [25]; while the δ for the packed bed reactor ranged from 0.07 to 0.25 at temperatures of 950–1120 °C respectively [36]. Otsuka et al. [21] studied the reaction mechanism between both doped and un-doped ceria for partial oxidation of methane (POM), where, the recombination or desorption of the produced H_2 was identified as the rate determining step for the reduction reaction. In a further study Otsuka et al. [37], reported activation energy of POM over pure ceria to a value around 160 kJ/mol. Warren et al. [38], in a recent work described the kinetic behaviour related to POM over pure ceria between 750 °C and 1100 °C using Arrhenius-type plots. The impact of different factors like the limitation of gas/solid diffusion, gas composition ratio between the reactant and the product, etc. were accommodated in the kinetic model. The activation energy reported was much lower than that reported by Otsuka, varying from 20 kJ/mol to 80 kJ/mol, with the higher value being obtained at a $\delta > 0.15$. Furthermore, a complete reduction of ceria was reported beyond 900 °C [38]. However, the study does not report the sample characterization and microstructure analysis to support the claim. Especially due to the fact, that ceria tends to change its crystal lattice structure above an oxygen loss of 17%, as is evident from the ceria phase diagram [39].

For the oxidation reaction, Le Gal and Abanades [40] studied and reported the kinetics of both water and CO_2 splitting from the perspective of solar fuel chemistry. For un-doped ceria, Le Gal et al. [41] adopted the second-order power law model via the "Master Plot" approach [42,43] to best describe the carbon dioxide splitting (CDS) kinetics. However, no kinetic parameters were reported. Arifin et al. [44], using a modified approach, separated the experimental effects from material specific H_2 and CO curve rates and reported the water splitting (WS) kinetics by a first-order kinetic model. A low apparent activation energy of 29 kJ/mol was obtained in the range of 750–900 °C. On the other hand, CDS kinetics was found to be surface-mediated phenomena with much higher complexity than the WS reaction. Therefore no one solid state kinetic model (SS) was obtained to accurately predict the CO yield over the entire range of experimental conditions of 600–875 °C. This is due to the fact that the SS models, essentially lumped parameter models with a minimal level of detail about the reaction mechanisms, does not account for the transient phenomena occurring during the CDS reactions. Farooqui et al. [45] in another recent study, tried to overcome this limitation with the identification of a proper kinetic model for the CDS reaction. The authors compared the different reaction models to experimental data (re-oxidation kinetics of ceria by CO_2 at a temperature range of 700–1100 °C) by curve fitting, followed by statistical comparison with the Residual sum of squares (RSS), Akaike information criterion (AICc) and the F test methods. The nested category model of nucleation and grain growth, the Sestak-Berggren (SB) was found to more suitable to fit the experimental data of the CDS reaction obtaining an activation energy of 79.1 ± 6.5 kJ/mol [45].

Nevertheless, the different experimental conditions, including experimental artifacts significantly affect the overall outcomes and hence the results of the experiments. This

Please cite this article as: Farooqui A et al., Assessment of integration of methane-reduced ceria chemical looping CO_2/H_2O splitting cycle to an oxy-fired power plant, International Journal of Hydrogen Energy, https://doi.org/10.1016/j.ijhydene.2019.12.182

not only results in a wide discrepancy in the reported results but also in developing a comprehensive model to best describe a reaction over a wide range of temperature and operating conditions. A detailed discussion in this regard has been reported by Scheffe et al. [46]. Unlike the model developed by Bulfin et al. [47] which comprehensively describes the solar thermal reduction of ceria, over a wide range of operating conditions. Also, none of the studies, to the best knowledge of the authors have considered a model based kinetic approach that reports the reaction kinetics of POM with ceria reduction. This model specifically benefits in the identification of the rate controlling mechanism, with the simultaneous assignment of parameters to the kinetic model, so as to predict the reactions within the operating regime to the closest approximation [44]. In addition, kinetics of re-oxidation of the reduced metal oxide with CO_2 is a temperature dependent surface phenomena, it would proceed significantly slower in comparison to water splitting reaction [9,44,48]. Therefore, for simultaneous splitting of water and CO_2, CDS would be the rate determining step. This is especially of significance while splitting flue gas directly from oxyfuel power plants, taking advantage of its high exit temperature from gas turbines to generate additional energy [2]. This claim is supported by Archishman et al. [49] wherein a thermodynamic analysis showed the formation of H_2 is thermodynamically favourable over that of CO at lower temperatures. Thus, in this work, experiments were evaluate a semi-empirical solid state kinetic model for methane reduction of commercial ceria followed by CDS reaction with CO_2 as an oxidizer while water splitting kinetic models were used from the literature [9,44]. Subsequently, in order to better predict the efficiency of the system, these kinetic models were then applied in a moving bed reactor model for reduction and oxidation in a chemical looping unit for an oxy-fired power plant which was previously studied based on a thermodynamic model [2].

It is believed that this work would provide a perspective on actual achievable system efficiencies of practical chemical looping CO_2/H_2O splitting cycles. Indeed, most studies, utilising thermodynamic equilibrium models for producing fuels such as methanol, dimethyl ether [50,51], jet fuels [52], naphtha [32,52,53], kerosene [53] etc. seem to predict ideal efficiencies, much higher than practically possible from heterogeneous thermochemical redox reactions.

Experimental section

A horizontal tubular reactor was used to carry out isothermal redox cycles of powders of commercial CeO_2 (Alfa Aesar (99.95% purity)) between 900 and 1100 °C. The experimental setup comprised a tubular reactor, a control unit, a gas delivery system and an online mass spectrometer for a real-time gas measurement. The complete experimental set-up is depicted in Fig. 2. A Quadrupole Mass Spectrometer (QMS) (Hiden Analytical Inc.) was used to analyse the gas composition. After crushing, the ceria sample was sieved to 32 μm for the experiments. The centre of the inner alumina tube of the reactor was embedded with 250 mg of ceria powder within alumina wool. The total gas flow rate was fixed at 120 Nml/min during both the reduction and the oxidation steps. During both the reduction and the oxidation, the mole fraction of the reactant gases (CH_4 and CO_2 respectively), were varied between 20% and 50%, balanced with argon.

Ceria was reduced with methane at a set-point temperature to assess the extent of ceria reduction in terms of the maximum non-stoichiometric capacity (δ) and hence develop the reduction reaction kinetics. Thereafter, the oxidation reaction was carried out at that same temperature to that of the reduction with different concentration (molar fractions) of carbon dioxide to develop the oxidation kinetics of ceria. The online mass spectrometer measured the resulting H_2 and CO during reduction and CO during the oxidation. Based on the reactivity data, different reaction mechanisms (i.e., reaction order, diffusion, geometrical contracting and nucleation models) were compared for the best-fitting kinetic model.

Each experiment comprised a four-step cycle. During reduction, a mixture of methane and argon in varying concentrations (20–50% vol. basis) was passed over the sample to evaluate the reduction kinetics. The readings of the QMS were observed to analyse for complete reduction of ceria. However, in the case of lower reaction rates at lower temperatures, the reactant gases were passes for 75 minutes to ensure enough reduction to study the corresponding oxidation. After the reduction step, the reactor was purged with pure argon. This step, generally 10 minutes long, was sometimes extended as per the measurements in the QMS to ensure complete removal of residual gaseous reactants and products of the previous cycle. Thereafter, oxidation reaction was performed with a mixture of argon and CO_2 in different concentrations (20–50% vol. basis). The reaction was continued until no further CO was detected by the QMS. The cycle was completed by pure Argon purging for approximately 10 min or until the quantitative gas analyser (QGA) reading was stable enough to begin the next cycle, whichever is earlier.

Isothermal redox cycles were performed between the temperature ranges of 900–1100 °C. It must be clarified that, although, H_2 and CO were measured during reduction, methane splitting (cracking) reaction (equation (4)) occurring above 1200 °C [54,55], would give erroneous results from the reading of the hydrogen measurements. This is due to the formation of H_2 and elementary solid carbon, being deposited inside the reactor. Indeed, this would be evident from the subsequent oxidation with CO_2, whereby the reaction kinetics would depend not only on the ceria oxidation but also on the Boudard reaction (equation (5)) resulting in a higher amount of CO.

$$CH_4 \rightarrow C(s) + 2H_2 \quad (4)$$

$$C(s) + CO_2 \rightarrow 2CO \quad (5)$$

Thermodynamically speaking, without methane cracking, the ideal H_2/CO ratio generated from the reduction reaction should always be 2, as also observed within the reported conditions [56]. However, to minimize discrepancy in the results, the measurements of CO both during the reduction and the oxidation cycle were considered for fitting the necessary kinetic model as per the following equations (6) and (7):

Please cite this article as: Farooqui A et al., Assessment of integration of methane-reduced ceria chemical looping CO_2/H_2O splitting cycle to an oxy-fired power plant, International Journal of Hydrogen Energy, https://doi.org/10.1016/j.ijhydene.2019.12.182

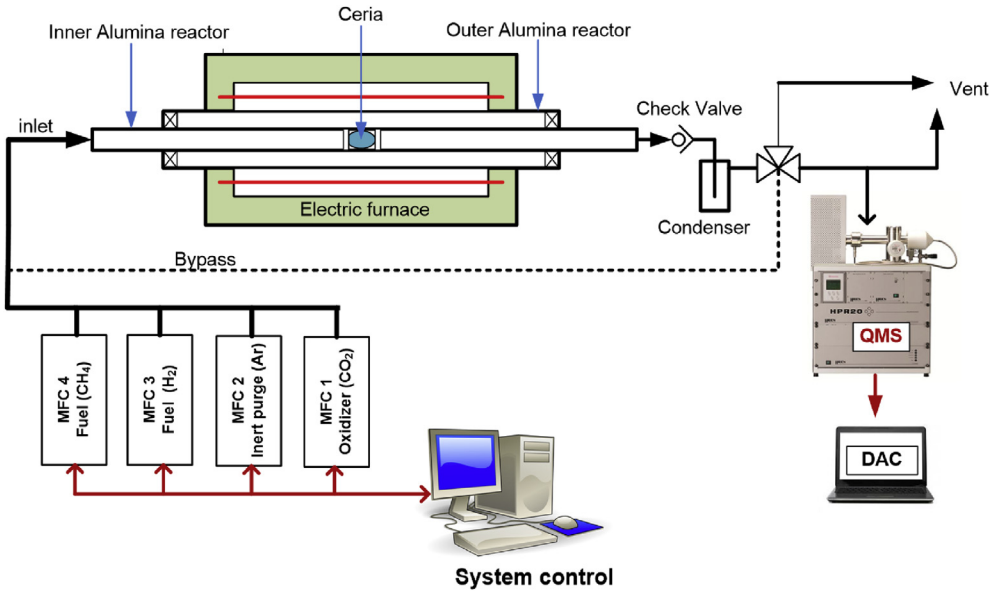

Fig. 2 – Experimental set-up for redox cycle testing in a horizontal tubular reactor configuration.

$$\dot{n}_{CO,RED} = \frac{X_{CO,out}\dot{n}_{RED,out}}{m_{CeO_2}} = \frac{X_{CO,out,RED}}{m_{CeO_2}} \frac{P^0 \dot{V}^0_{RED,in}}{RT^0} \quad (6)$$

$$\dot{n}_{CO,oxd} = \frac{X_{CO,out,OXI}\dot{n}_{OXI,out}}{m_{CeO_2}} = \frac{X_{CO,out,OXI}}{m_{CeO_2}} \frac{P^0 \dot{V}^0_{OXI,in}}{RT^0} \quad (7)$$

where $\dot{n}_{CO,RED}$ and $\dot{n}_{CO,OXI}$ are the flow rates of CO produced during reduction and oxidation respectively. $X_{CO,out}$ is the mole fraction of CO, as measured at the exit of the reactor, $\dot{n}_{out}$ is the molar rate of the gas mixture flowing from the reduction and oxidation reactor respectively, while T^0, P^0 and V^0 are the temperature, pressure and the total volumetric inflow rate at standard temperature and pressure (STP). The measurement of the reaction rates were conducted after normalization of both the reduction and oxidation steps by the total ceria sample m_{CeO_2} i.e. 250 mg. Since a quasi-steady-state was assumed during the experiments, no accumulation or depletion effect in the control volume was considered. This can be argued with respect to the negligible residence time of the gases in relation to the characteristic time of the redox conversion.

The change in the non-stoichiometry of ceria in the bulk phase was evaluated through the extrapolated reduction rate, according to the following equation (8). Correspondingly, the change in non-stoichiometry during oxidation was evaluated by extrapolating the oxidation reaction rate based on oxidation with carbon dioxide, given by the following equation (9).

$$\delta_1 CH_4(g) + CeO_2 \rightarrow \delta_1[CO(g) + 2H_2(g)] + CeO_{2-\delta_1} \quad (8)$$

$$CO_2(g) + \frac{1}{\delta}CeO_{2-\delta_1} \rightarrow CO(g) + \frac{1}{\delta}CeO_{2-\delta_2} \quad (9)$$

where, δ_1 and δ_2 correspond to the non-stoichiometry following the reduction and oxidation step respectively. The bulk phase change of non-stoichiometry over the entire redox cycle, $\delta = \delta_1 - \delta_2$ is calculated as per the following equation (Eq. (10)) [45]:

$$\delta(t) = \frac{n_{oxygen}(t)}{n_{CeO_2}} \quad (10)$$

where $n_{oxygen}(t) = \int_0^t \dot{n}_{CO_{RED}} dt = \int_0^t \dot{n}_{CO_{OXI}} dt$ represents the accumulated release and intake of oxygen ions resulting from the reduction and the oxidation reactions respectively, $n_{CeO_2} = m_{CeO_2}/M_{CeO_2}$ is the moles of ceria, with M_{CeO_2} as its molar mass.

The oxygen released and accepted by the metal oxide when reduced by methane and oxidized with CO_2 provides the measure of the non-stoichiometry, starting from a neutral state. Therefore, after oxidation, alternatively the completion of one cycle, the oxygen vacancies are saturated inside the metal oxide. Temperature is one of the most influential factors affecting the maximum non-stoichiometry, where, an increase in temperature results in an increased rate of oxygen release and hence, increased the availability of vacancies.

Material characterization

X-ray diffraction (XRD), using a PANalytical X'pert MPD Pro diffractometer with Ni-filtered Cu Kα irradiation (wavelength 1.5406 Å) was used to investigate the change in the lattice structure of the samples before and after the reduction cycles, and hence their structural integrity. A step size of 0.2°/s in the 2θ range from 5° to 145° was used to scan all samples. The crystallite size of samples was calculated from the Scherrer equation (equation (11)) based on the reflection with the highest intensity for a rough estimation on sintering effect, during the experiment.

$$D = \frac{0.9\lambda}{\beta \cos\theta} \quad (11)$$

Please cite this article as: Farooqui A et al., Assessment of integration of methane-reduced ceria chemical looping CO_2/H_2O splitting cycle to an oxy-fired power plant, International Journal of Hydrogen Energy, https://doi.org/10.1016/j.ijhydene.2019.12.182

here θ is the Bragg's angle which is needed to evaluate β (width at half maximum intensity) at a wavelength of λ to determine the grain size (D). Crystallite micrographs were obtained at an accelerating voltage of 5 kV under a scanning electron microscope (SEM, JSM7800F).

Reactivity results

Production rate (ml/min/g) and the total yield (ml/g) of the product gases (CO and H_2 during reduction and CO during oxidation) were investigated. However, as per the discussions presented in Section Experimental Section, to reduce errors in the measurement and prediction of the performance of the both the POM and CDS reactions over commercial ceria, CO production rate and total yield of CO was utilised to develop kinetics for both the redox reactions. Furthermore, to achieve the desired results, i.e., attain a reliable fitted kinetic model of methane reduction of commercial ceria and corresponding oxidation with CO_2, five consecutive redox cycles were performed to attain stable results. As can be observed from Fig. 3, except the first cycle, all the other cycles show consistent repeatability for both the oxidation and the reduction reactions. For the kinetic analysis, the fifth cycle is taken into consideration.

Effect of temperature

Fig. 4 shows the effect of temperature on the CO production rate for both the reduction and oxidation reactions between 900 and 1100 °C. As can be observed from each plot, the reaction rate is characterized by a slow initial stage, a fast-middle stage, also resulting in a peak reaction rate, with a subsequent drop in production rate. During reduction, the slow increase in the CO release results from the release of oxygen from the crystal lattice of the metal oxide.

A significant variation in both the relative length of each of the three phases, as well as the peak reaction rate occurs with varying the reduction temperature. However, the impact of temperature is much more pronounced on the peak production rate, as can be seen from Fig. 4(a). Indeed, notwithstanding an increase in the total product yield with a rise in temperature, the overall reaction rate significantly increases with sharper and narrower peaks at a higher temperature. For example, as the temperature increases from 950 °C to 1100 °C, the peak production rate of CO was observed to increase by almost six times. The most marked rise in the production rate occurred between 1000 °C and 1050 °C, when it almost tripled. Also, with temperature, the peak production rate becomes faster and quicker (around 600 seconds for 950/1000 °C and around 400 s for 1050 °C). After the peak, the production rate drops rapidly, with a complete reaction taking place in around 1000s for all temperatures above 900 °C. At 900 °C, no significant peak is even noticed, with a flatter trajectory occurring over a larger time due to the lower amount of available oxygen sites. Such low temperatures therefore indicate an extremely slow reaction rate, which would hence limit the overall non-stoichiometric ceria conversion.

On the other hand, for the oxidation reaction, a rapid rise in the CO yield is observed due to the rapid oxygen vacancies ion incorporation. Similar to the reduction reaction, after peak production rate of CO which drops sharply approaching zero in 80–150 s, for all temperatures. It needs to be mentioned here that the performance of the oxidation reaction is directly influenced by the net non-stoichiometry generated in the reduction step at temperatures below 1100 °C. At temperatures above 1100 °C, due to increase in methane cracking, elementary solid carbon would be deposited inside the

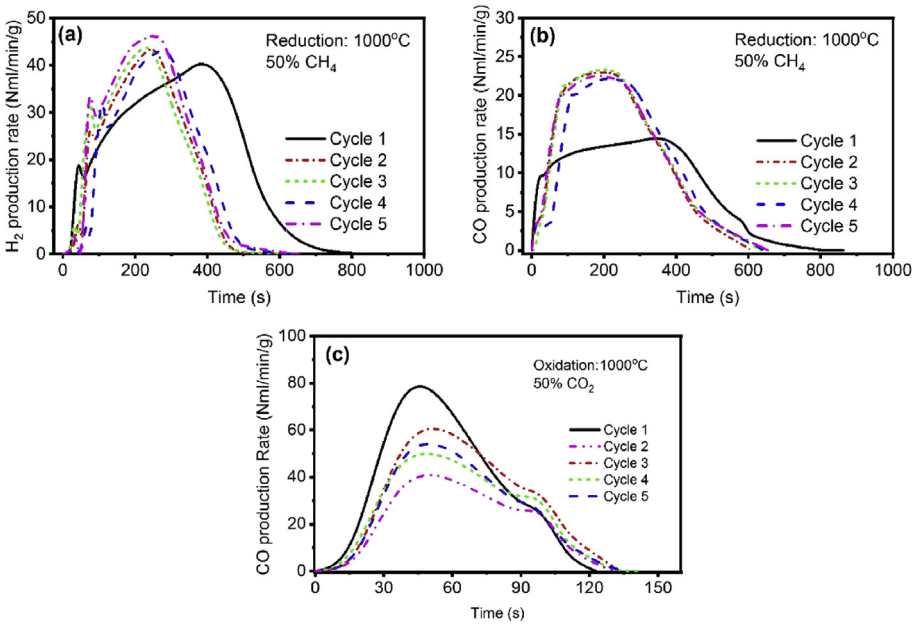

Fig. 3 – (a) H_2 and (b) CO production rate from the reduction of CeO_2 over 50% CH_4 and (c) oxidation of the reduced metal oxide with 50% CO_2 over five cycles each.

Please cite this article as: Farooqui A et al., Assessment of integration of methane-reduced ceria chemical looping CO_2/H_2O splitting cycle to an oxy-fired power plant, International Journal of Hydrogen Energy, https://doi.org/10.1016/j.ijhydene.2019.12.182

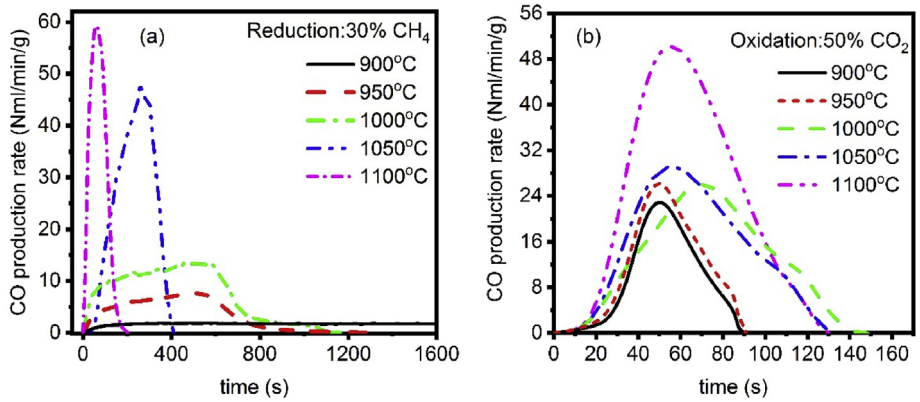

Fig. 4 – Variation of yield rates of CO in (a) reduction and (b) oxidation of CeO_2 in the redox cycle of methane reduction followed by oxidation with CO_2 with the variation of temperature in the range 900 °C and 1100 °C; Methane concentration during reduction: 30%; CO_2 concentration during oxidation: 50%, baseline reactor pressure: 1 atm.

reactor. This is especially problematic, above 700 °C, as the Boudard reaction becomes spontaneous [57], producing CO through gasification of elementary carbon by CO_2. This would therefore not only considerably influence the overall CO production rate, but also increase its overall CO yield under sufficient availability of CO_2. Indeed, this can be observed in Fig. 4(b). With the production rate and yield of CO considerably different at 1100 °C to that of the temperatures below it, an indication of methane cracking during reduction at 1100 °C could be predicted. This hypothesis was later justified by microstructure analysis, presented in Section Microstructural analysis and it identifies the reduction reactor in the oxi-fired power plant layout. Nonetheless, for temperatures below 1100 °C, a lower non-stoichiometry during reduction would reduce the overall ceria oxidation reaction time as well. Thus, a significantly lower time of oxidation was observed at 900 °C ($\delta = 0.10$) than at 1050 °C ($\delta = 0.23$). However, as can be observed from Fig. 4(b), CO peak increases and broadens with increase in the temperature, indicating the presence of a higher activation barrier towards CO_2 splitting [58]. Similar results of strong temperature dependence of CO_2 splitting observed in the present study have been reported in earlier literature as well [59–61].

Effect of concentration

The influence of the concentration of the reactants on the reduction and the oxidation kinetics of ceria with methane and CO_2 respectively was also investigated and represented in Fig. 5. A decrease in the reaction time for both the reduction and the oxidation with an increase in the partial pressure of CH_4 and CO_2 in the feed respectively was obtained. This was accompanied by a higher CO production rate. Similar effects from lower activation energies at higher CH_4 concentration during fuel based reduction was reported by Warren et al. [38] and Zhao et al. [62]. For oxidation, Farooqui et al. [45] also reported similar reaction trends.

An increase in the reaction rate, however, is counterbalanced by a decrease in the reaction time. Therefore, at a given temperature, the net yield of CO during the reduction and oxidation reactions remains fairly constant. For instance, for the reduction at 1000 °C, although the maximum non-stoichiometry generated at lower (30% CH_4, balance Argon) and higher (50% CH_4, balance Argon) methane concentrations was 0.20, and 0.184 respectively, the overall net yield of CO during oxidation corresponded to that during reduction. This

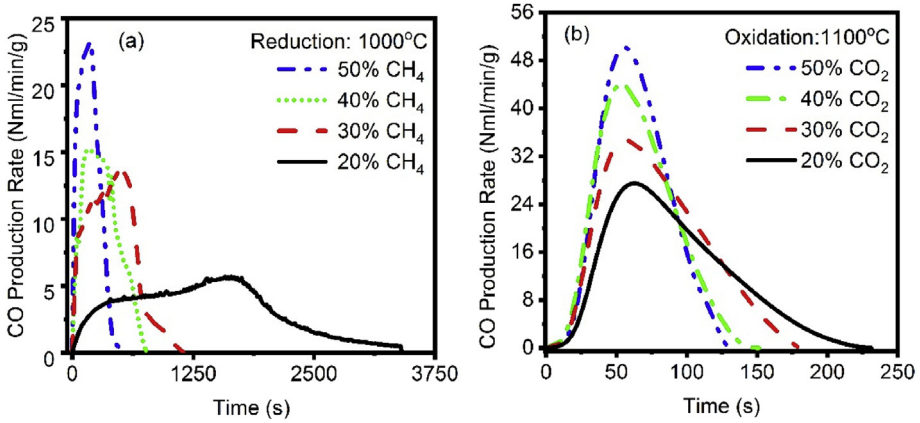

Fig. 5 – Variation of yield rates of CO in (a) methane reduction of ceria at 1000 °C and (b) oxidation of reduced ceria at 1100 °C with the variation of concentration of the gaseous reactants at a reactor pressure of 1 atm.

Please cite this article as: Farooqui A et al., Assessment of integration of methane-reduced ceria chemical looping CO_2/H_2O splitting cycle to an oxy-fired power plant, International Journal of Hydrogen Energy, https://doi.org/10.1016/j.ijhydene.2019.12.182

therefore clearly indicates the result in the complete oxidation of ceria.

Fig. 5(a), also shows that the peak production rate considerably shifts to a lower time with rising methane concentrations. While for 50% methane concentration, the peak CO production rate is noticed at about 200 s, the CO production rate peaked after 1750 s with 20% methane in feed. In contrary, the oxidation reaction, does not show such a significant impact of the variation of concentration, as can be noticed from Fig. 5(b). The peak production rate is registered in the range of 60–70 s. In relation to the peak rate variation with concentration of feed, the variation was non-linear for the reduction reaction (Fig. 5(a)). However for the oxidation, linear rise in the peak reaction rate with the concentration of CO_2 in the feed is observed. The lower dependence of CO_2 splitting on the concentration of the CO_2 in the feed in comparison to methane for reduction has been reported elsewhere as well [7,45,60,63].

Fig. 6 shows the CO peak production rate and total yield of CO from the reduction of ceria by methane and oxidation by CO_2 for different temperature and concentration of interest, and as per the experimental conditions stated above. As can be seen from Fig. 6(a), the concentration of oxygen vacancies in the ceria increases with temperature from 900 up to 1050 °C. This can be followed from the increase in the total CO yield from 37.7 to 84.5 ml/g between 900 °C and 1050 °C, resulting in an increase in the non-stoichiometry (δ) of ceria from 0.1 to 0.23. Similar non-stoichiometry is reported by Warren et al. [36], where a δ of 0.21 was obtained at 1035 °C. It is worth mentioning that the peak CO production rate for lower temperature are very low, for example 2 ml/min/g at 900 °C. This was countered by making the reduction step sufficiently long to ensure sufficient reduction of ceria. Thus, a 62 minute reduction step was accounted for at 900 °C as compared to that at 1000 °C, which lasted for only 19.5 minutes with a peak CO production rate of 14.2 ml/min/g. At 1100 °C the CO yield during reduction significantly drops to 47.9 ml/g, resulting in a reduced δ of only 0.12.

Higher concentration of methane, however is deterrent to the oxygen carrying capacity of ceria during reduction. This is evident from Fig. 6(b), whereby, the total CO production decreases from 90.7 to 34.0 ml/g (δ = 0.24–0.17) as the methane concentration increased from 20% to 50% at 1000 °C. However, the corresponding peak CO production rate increased from 5.8 to 23.8 ml/min/g. Nonetheless, the decrease of total CO production can be explained by the fact, that at higher methane concentrations, an increased carbon deposition occurs at the surface of the sample, blocking sites with potentially available oxygen. Similar results have been previously reported by Chuayboon et al. [64].

The variation in the total CO production yield and peak production rates with temperature during the oxidation of reduced ceria with CO_2 is obtained from Fig. 6(c). Generally speaking, the oxidation reaction can be observed to be fairly fast. Indeed, more than 70% of the overall δ change occurred within the first 20s of the oxidation reaction. A steady increase in the CO yield between 900 and 1050 °C from 12.7 to 23.8 ml/g can be attributed to the increased non-stoichiometry generated from the corresponding reduction (δ = 0.1–0.23). However, in contrast to the drop in reduction extent of ceria at 1100 °C, the total CO production during oxidation at 1100 °C increases considerably. This rise could be explained considering the Boudard reaction (Eq. (5)) to be active due the formation of carbon from methane splitting during corresponding reduction reaction at 1100 °C. Therefore, although a faster reaction is achieved at higher temperatures,

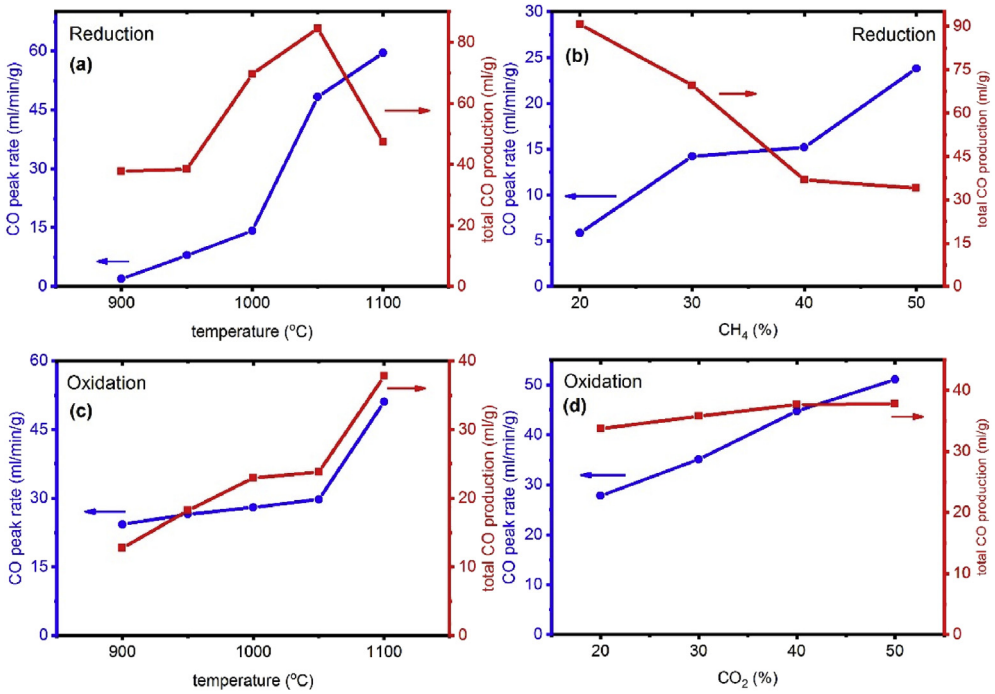

Fig. 6 – CO peak rate and total CO production for varying temperatures and feed concentrations with CH_4 of 30% and CO_2 of 50% during reduction and oxidation respectively, T = 1100 °C during oxidation.

Please cite this article as: Farooqui A et al., Assessment of integration of methane-reduced ceria chemical looping CO_2/H_2O splitting cycle to an oxy-fired power plant, International Journal of Hydrogen Energy, https://doi.org/10.1016/j.ijhydene.2019.12.182

methane cracking would limit the increasing of operation temperatures beyond 1050 °C.

Minimal impact of the molar fraction of CO_2 in the feed was observed for ensuring the complete conversion of the reduced ceria during oxidation,; whence the total CO production ranges only from 33.7 ml/g to 37.8 ml/g while varying CO_2 molar fraction from 20% to 50%. However a higher CO_2 molar fraction ensured a faster reaction, as the peak CO production rate increased from 27 to 51 ml/min/g.

It is important to mention that methane reduction kinetics is much slower than that of the most commonly studied H_2 reduction. Similar results of CO production rates are reported by Zhou [65] for methane reduction for lower temperatures. However, followed by oxidation of reduced-ceria oxidation with H_2O. As for the oxidation with CO_2, CO yield was obtained to be higher for similar CO_2 concentration during the corresponding oxidation step of hydrogen reduced ceria. For instance, a CO yield of 28.5 ml/g was reported by Ref. [45] while oxidising H_2 reduced ceria with 20% CO_2, compared to 33.7 ml/g reported in the present study with CH_4 reduction.

Microstructural analysis

XRD patterns of ceria before and after the reaction cycles for different temperatures (Fig. S1 supporting information file), reveal a cubic fluorite structure of ceria in all the conditions used. Compared to XRD patterns before cycling, the peaks appear more intense after cycling, which indicates an improvement of crystallinity (decrease of microstrains and growth of grain) due to the thermal treatment at high temperature. From Scherrer equation (as explained in experimental section) a crystal size of 117 nm was evaluated. Comparing with an initial grain size (larger than 80 nm), XRD peak width cannot give information regarding the growth of crystal size due to the increment of operating temperature. In general, for size higher than 100 nm the instrument contribution to the peak width overwhelms the signal from the crystallite size broadening and it is not possible to determine this latter contribution [66].

SEM characterization helps more to define the splitting processes within the operating conditioning. With 30% CH_4 concentration during reduction at 900 °C, ceria was found to be present in particles of 60–100 nm, which would often form bigger aggregates of 2 microns as shown in Fig. 7(a,b). In Fig. S2 (a) evidence of the presence of a rod of SiO_2 can also be detected. This could be from the quartz wool sheets used to support/block the catalyst in the reactor. The threshold temperature to fasten the deactivation processes is 1000 °C as shown in Fig. S3 in supplementary file. The size of aggregates of ceria at 1000 °C slightly increase with respect to that of the samples treated at 900 °C and increases more with the number of cycles. (Fig. S3 (a) and (b)). Moreover a few carbon deposits in form of sheet can also be observed, mostly coating the SiO_2 rods. However, when the methane is fed in higher concentration the carbon deposit is more evident and result covering with small sheets also the ceria aggregates (Fig. S3 (c) and (d)). However, carbon coating over ceria is not homogeneous. At higher temperature of 1100 °C, the carbon is rarely observed on the sample, however, the ceria aggregates resulted very compact with size varies from 3 microns to 30 microns (Fig. 7 (c) and (d)). The observation of carbon deposits at high temperature and with high concentration of methane justify the drop of CO yield during reduction (Fig. 6(a)) and its corresponding rise during oxidation. The carbon formed during

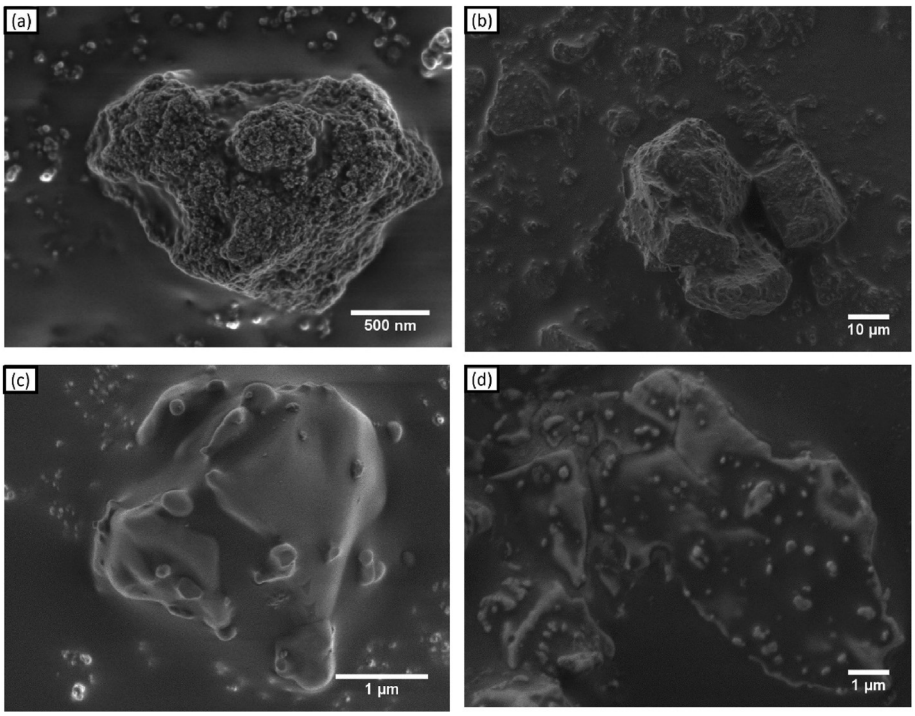

Fig. 7 – Phases, and compositions in the samples of ceria tested at (a) 900 °C (b) 1000 °C (c) 1100 °C at 30% CH_4 (d) 1000 °C at 50% CH_4.

Please cite this article as: Farooqui A et al., Assessment of integration of methane-reduced ceria chemical looping CO_2/H_2O splitting cycle to an oxy-fired power plant, International Journal of Hydrogen Energy, https://doi.org/10.1016/j.ijhydene.2019.12.182

methane splitting undergoes the Bourdard reaction forming CO at a higher temperature, with the process being further possibly catalysed by CeO_2.

The above observations are also reported in literature. Carbon deposition for methane reduction of ceria at over 1100 °C and for a δ of over 0.2 has been reported by Otsuka et al. [21,37]. Furthermore, methane cracking has also been reported to be enhanced at temperatures above 1100 °C in the presence of alumina (Al_2O_3) [67], which is also the material of the present reactor. As an alternative, Warren et al. [38], suggests the use of platinum crucible. In addition, the passing of excess amount of methane or excessive residence times could also lead to significant carbon deposition, even though not considered as conditions in the present set of experiments [68].

Kinetic study

The kinetic model parameters were evaluated based on the iso-conversion and isothermal reaction analysis [69]. Model fitting of the experimental data to identify the solid-state reaction kinetic mechanistic model for both the reduction and oxidation of ceria was employed to evaluate the reaction kinetics. Reaction rate, defined as the time profile of reactant conversion was adopted as the metric for comparison of reaction models [70]. The different solid-state reaction kinetic models compared in the present study are compiled in Table S1 in the supplementary file.

The reaction extent was obtained from the solid conversion (X). Following the above discussions, as CO was chosen to be the common concerned product irrespective of the reduction and oxidation reactions, the following equation (12) remains valid irrespective of the type of experiment performed.

For each time instant, t_i, the instantaneous conversion $X(t_i)$ can be given by the ratio between the ith value of the cumulative to the overall cumulated value.

$$X(t_i) = \frac{\int_{t=0}^{t=t_i} n_i \cdot dt}{n_{itot}} \tag{12}$$

Essentially, this fixes the overall conversion, X to vary between 0 and 1, n_i is the instantaneous quantity of the product i, n_{itot} is the total quantity of the product i if the reaction reached equilibrium state. The kinetic model for the gas-solid reaction can hence be described through a mathematical equation as per the following equation (13) [71]:

$$\frac{dX}{dt} = k_1 \cdot f(X) \cdot [P]^m \tag{13}$$

where X represents the conversion, $k_1 = A\exp(-E_a/RT)$ and P is the partial pressure of the gas phase reactants (CH_4 or CO_2); m is the reaction order and f(X) is the function of X following the reaction mechanism. Here A and E_a are the Arrhenius parameters, A being the pre-exponential factor and E_a the activation energy. R is the universal gas constant is 8.314 J/mol/K.

At first, model fitting was performed to the raw data, for which, Eq. (13) was re-written as the following equation (14):

$$\frac{dX}{f(X)} = K \cdot dt \tag{14}$$

here $K = k^1 \cdot P^m$ is expressed as a function of the partial pressure of the gas phase reactants. By the integrating equation (14) over the complete reaction extent, it can be subsequently expressed as equations (15) and (16).

$$g(X) = \int_0^X \frac{dX}{f(X)} \tag{15}$$

$$g(X) = K \cdot t \tag{16}$$

K is obtained as the slope of the g(X) vs t curve, whereas, the negative slope between the natural log of K vs 1/T gives the activation energy, as per equation (17). On the other hand, the intercept of the plot between $\ln(AP^m)$ with P is the partial pressure of the gas phase reactants. The reaction order could hence be calculated by plotting $\ln(AP^m)$ vs. lnP after equation (18) with the slope providing the reaction order and the intercept, the 'A' value.

$$\ln K = -\frac{E_a}{RT} + \ln A \cdot P^m \tag{17}$$

$$\ln[A \cdot P^m] = \ln A + m \ln P \tag{18}$$

Finally, the kinetic expressions of the models reported in Table S1 in the supplementary file were matched with the experimental data obtained by evaluating dX/dt vs X profiles. For this, the value of the K parameter was fitted and correspondingly, the model with the least residual sum of squares (RSS) and R^2 close to unity was selected to be the best fit for the present reaction.

Kinetic parameter evaluation

Based on the models listed in Table S1 in the supplementary file, a comprehensive evaluation with all the models was performed, together with finding the least RSS by fitting each model to the experimental results. Of them, the Avrami-Erofe'ev (AE3) model that considers nucleation and grain growth was found to fit best with the experimental results for both the reduction and oxidation reactions. The following section summarizes the kinetic results of the two redox reactions of ceria.

Ceria reduction by methane

As mentioned, based on the calculation of the least errors of all the models fitted to the experimental results, an average R^2 value of 0.97 was obtained for the AE3 model, showing a good match.

The kinetic parameters were evaluated post the selection of the kinetic mode as per the procedure explained above through equations (17) and (18). The plots between $\ln(A \cdot P^m)$ vs ln(P) and ln (K) vs 1/T for the reduction reaction are shown in Fig. 8. A reaction order of 2.0 ± 0.36 was obtained. Fig. 8 (a) represents the ln(K) vs (1/T) plot reduction of ceria with 30% methane, corresponding to which, the average activation energy was calculated as $E_{RED\text{-}CH4}$ = 283.65 ± 0.66 kJ/mol with higher than 95% confidence level. The pre-exponential factor, $A_{RED\text{-}CH4}$ was calculated as 8.67E9 ± 433 s^{-1}.

The concentration effect in terms of reaction order was further evaluated through curve fitting and was obtained to

Please cite this article as: Farooqui A et al., Assessment of integration of methane-reduced ceria chemical looping CO_2/H_2O splitting cycle to an oxy-fired power plant, International Journal of Hydrogen Energy, https://doi.org/10.1016/j.ijhydene.2019.12.182

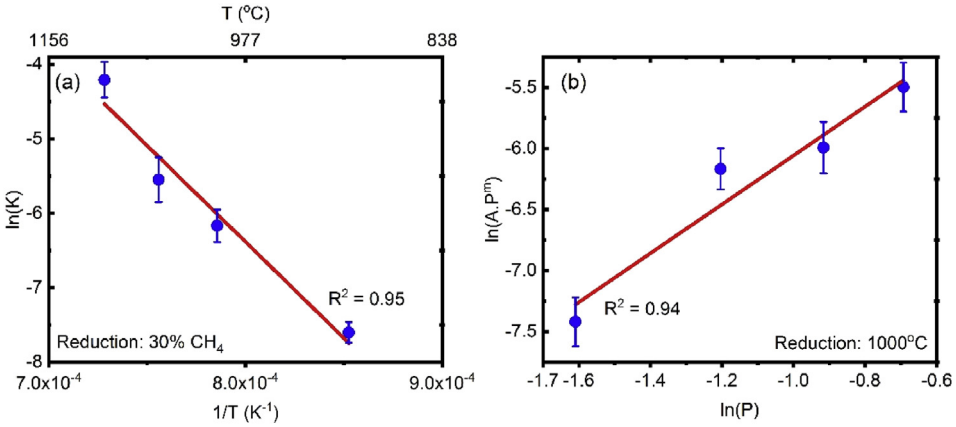

Fig. 8 – (a) ln(K) vs (1/T) of the reduction reaction considering Avrami Erofe'ev AE3 model; (b) ln(AP^m) vs ln(P) plot for reduction reaction order determination.

vary both with temperature and concentration. In this regard, a regression analysis between m_{RED}, T and P in terms of concentration was carried out for temperatures below 1050 °C using statistical methods. The relation obtained is described by the following equation (19) and the corresponding R^2 value obtained was 0.98. Beyond 1050 °C, the reaction order was found to remain constant at 2.2.

$$m_{RED} = 19.897 - 0.013 \times [T] - 1.28 \times [P_{CH_4}] \quad (19)$$

where T is in Kelvin and P is the concentration or partial pressure of the gaseous reactant, considering ideal gas laws.

The value of activation energy and the other constants obtained in the model fit well to the experimental results, as obtained through curve fitting using the proposed model and shown in Fig. 9. Although a slight over-estimation and under-estimation for lower and higher concentrations is predicted by the developed model, a good agreement of the results both with respect to concentration and temperature variation can be seen. Compared to existing literature, the activation energy obtained in the present study, 283.65 ± 0.66 kJ/mol, lies within the range of 20 kJ/mol to 334.56 kJ/mol [26,38,72] reported for a variety of temperature and reactant concentration during reduction. Warren et al. [38] reported that the activation energy varies between 20 and 80 kJ/mol as the non-stoichiometry (ranges from 0 to 0.35). Otsuka et al. [37] reported 160 kJ/mol of activation of methane reduction by ceria with Pt as a catalyst. A similar value of activation energy of 165–176 kJ/mol is reported by Ramirez Cabrera et al. [22] while investigating the effect of doping of Gd and Nb over ceria. It is observed that the activation energies are reduced by the doping or by using a catalyst with the ceria. The activation energy estimated in the present experiments are higher than reported by Le Gal et al. [40] (221 kJ/mol) and lower than that reported by Ackermann et al. [72] (344.56 kJ/mol) which was evaluated for considering oxygen diffusion in ceria. In spite of all the results lying within the 95% confidence level, due to the large variation in the reported activation energy values, no comprehensive comparison with literature data can be done.

$CeO_{2-\delta}$ oxidation by CO_2

Like the reduction reaction, a similar curve fitting was performed using least square of errors on all the models listed in Table S1 in supplementary file. As like the reduction reaction,

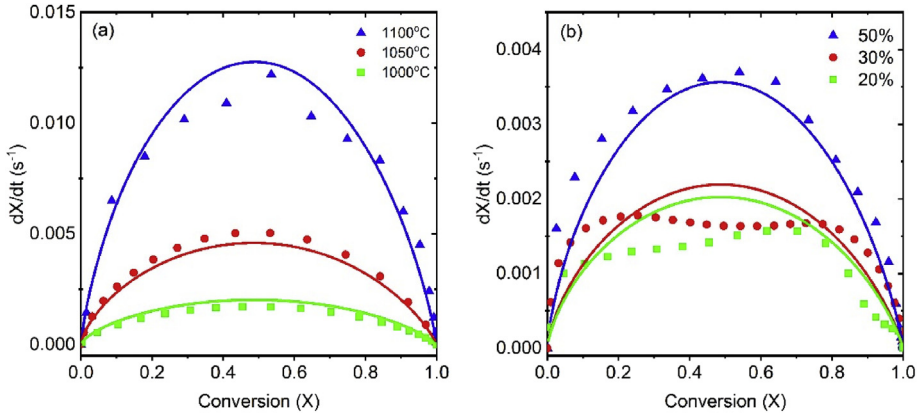

Fig. 9 – Comparison of the kinetic model and the experimental data for methane reduction of ceria (a) with the variation in temperature, 1000 °C, 1050 °C, 1100 °C and (b) with the concentration of CH_4 of 20%, 30% and 50% for reactor pressure of 1 atm. The symbol represents experimental data and lines represent the kinetic model.

Please cite this article as: Farooqui A et al., Assessment of integration of methane-reduced ceria chemical looping CO_2/H_2O splitting cycle to an oxy-fired power plant, International Journal of Hydrogen Energy, https://doi.org/10.1016/j.ijhydene.2019.12.182

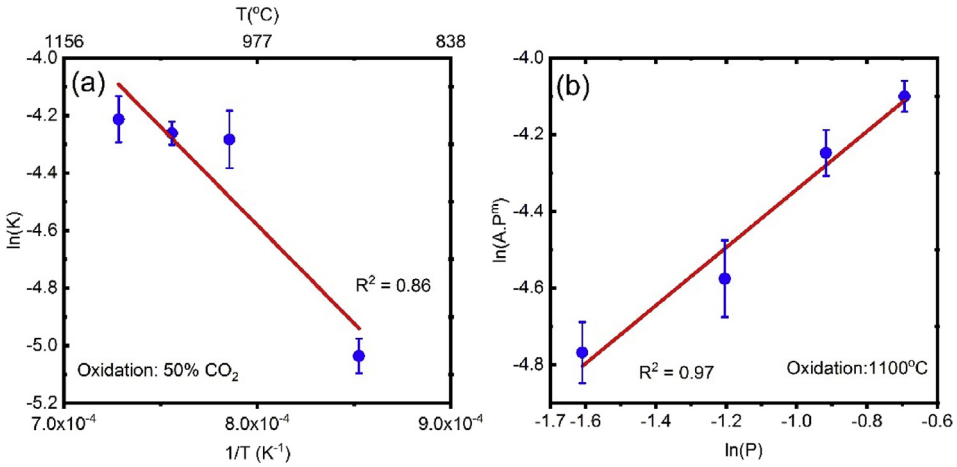

Fig. 10 – (a) ln(K) vs (1/T) Arrhenius plot of the oxidation reaction for AE3 model; (b) ln(AP^m) vs ln(P) plot for reduction reaction order determination.

the AE3 model fits best with the experimental results and the average R^2 value obtained was 0.98, showing a good match.

Using the similar procedure as that of reduction, the reaction order of the oxidation reaction was obtained as 0.732 ± 0.186 with an R^2 of 0.97, as can be seen from Fig. 10(b). Correspondingly, Fig. 10(a) represents the ln(K) vs (1/T) plot oxidation with 50% CO_2, following which, the average activation energy was calculated as $E_{OXI\text{-}CO2}$ 59.68 ± 6.09 kJ/mol and the pre-exponential factor, $A_{OXI\text{-}CO2}$ of 64.48 ± 1.45 s^{-1}.

In an equivalent manner, the concentration effect in terms of reactor order was obtained to vary both with temperature and concentration. A regression analysis between m_{OXI}, T, and P in terms of concentration was carried out for all temperatures and concentrations using statistical methods. The relation obtained is described by the following equation (20) and the corresponding R^2 value obtained was 0.985.

$$m_{OXI} = 0.002 \times [T] - 7.5 \times [P_{CO_2}] - 1.996 \quad (20)$$

Similar validation studies were performed with the model fit and the experimental results. The values obtained match closely with the results presented by Farooqui et al. [45] for oxidation of ceria following hydrogen reduction, where the activation energy obtained was 79 kJ/mol [45]. Furthermore, curve fitting using the obtained value was performed and presented in the following Fig. 11. Since the non-stoichiometry of reduction increases with the increase in temperature, it would be empirical to fix non-stoichiometry of particular value to compare the reaction rate. Therefore reaction rate data of the model is compared with the experiments for those conditions in which δ_{red} reached 0.22. A good agreement of the results, both with respect to concentration and temperature variation can be seen. A slight overestimation for lower CO_2 concentrations are obtained like reduction. However, for higher CO_2 concentrations a very good fit can be seen with an overall confidence level more than 95%, while agreeing well to the values obtained in similar studies performed reported in the literature.

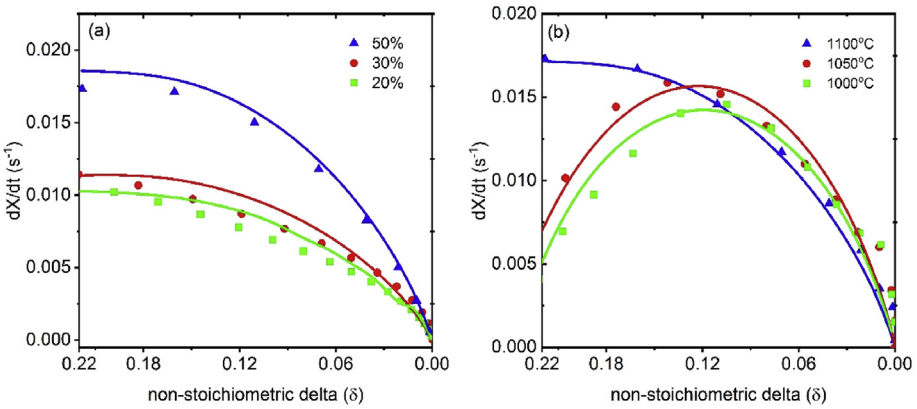

Fig. 11 – Relative fit of the kinetic model to the experimental data for oxidation of reduced ceria with CO_2 (a) with the variation in concentration of CO_2 of 50%, 30% and 20% (b) with temperature of 1000 °C, 1050 °C, 1100 °C for reactor pressure of 1 atm and a constant non-stoichiometric extent of reduced ceria of 0.22. The symbol represents experimental data and lines represent the kinetic model.

Please cite this article as: Farooqui A et al., Assessment of integration of methane-reduced ceria chemical looping CO_2/H_2O splitting cycle to an oxy-fired power plant, International Journal of Hydrogen Energy, https://doi.org/10.1016/j.ijhydene.2019.12.182

Effect of kinetics of methane-driven CL unit and its integration to an oxy-fuel NGCC with CO_2 recycling via splitting (OXY-NGCC-CL)

In an earlier work, the authors proposed a 500 MW oxyfuel power plant integrated with the chemical looping CO_2/H_2O splitting unit for recycling of a fraction of the exhaust gas to generate additional electricity [2]. The process flow diagram can be seen in Fig. 12. Based on the thermodynamic assessment, an energetic efficiency of 51.4% was obtained, an improvement of almost 7% to that of the state-of-the-art oxyfuel NGCC with 100% carbon capture. However, as the ceria undergoes a highly non-stoichiometric reduction, a realistic analysis would require the kinetic assessment of the chemical looping splitting (CL) unit. Indeed, this would therefore necessitate re-evaluating the performance of the proposed layout. Before developing the kinetic model of the CL unit, a brief description of the power plant layout proposed earlier [2] is described below.

Acknowledging the difficulty in significant retrofits required to incorporate the chemical looping splitting cycle in an oxy-fuel power plant, a novel natural gas fired power plant with 100% was conceived [2]. An air separation unit (ASU) would supply the O_2 necessary for combustion. The primary fuel to the plant, natural gas, would be fed to the reduction reactor (RED) of the CL unit, where syngas is generated while reducing ceria. The syngas from the RED is combusted in the oxyfuel combustor aided by a fraction of recycled CO_2, to maintain the outlet gas temperature from the combustor to the turbine inlet temperature (TIT). Following expansion in the gas turbine, a part of the exhaust gas mixture (CO_2/H_2O) would be sent to the oxidation reactor (OXI) of the CL unit. In the OXI, additional syngas would be generated, which is subsequently used for additional power generation via a secondary oxy-combustion combined cycle. As the exhaust gases from the gas turbines are at high temperatures, high-temperature steam for the bottoming Rankine cycle could be generated via a heat recovery steam generator (HSRG). The oxy-combustion further ensures minimal SO_x and NO_x, therefore allowing the exhaust gases to be cooled down to 50 °C with a large heat recovery. The remaining CO_2, following separation for recirculation into combustion chambers, is sent for storage after compression of 110 bar. Additionally, substantial heat could be recovered from both streams of syngas from the CL unit from the cool-down before compression, which would allow for additional steam generation, and hence potentially increasing the efficiency of the proposed plant.

The primary component of the proposed layout is chemical looping (CO_2/H_2O) unit (CL). Pre-cleaned natural gas is first preheated and then expanded to the working pressure of the reduction reactor through a turboexpander (TURBEXP). The expanded and pre-heated natural gas is supplied to the reduction reactor (RED) where it undergoes partial oxidation of methane (POM) producing syngas. The operating conditions were selected based on the experiments and to avoid methane cracking. Thus a reduction temperature of 1000 °C was considered ideal. Since a supplemental heat is required for reduction reactor an heat integration of combustion chamber of the power plant and reduction reactor is proposed with annular reactor design with inner reactor being reduction reactor of CL unit and annulus being combustion chamber providing excess heat [73]. More details of the system layout equipment operating conditions can be obtained from Ref. [2] with the assumptions listed in Table S2 in supplementary file.

Moving bed methane-driven chemical looping CO_2/H_2O splitting model

Fig. 13 represents the schematic of a counter-flow moving bed model for reduction and oxidation reactor. In the reduction reactor (RED), ceria is introduced from the top by a hopper system (not shown) and it is reduced by incoming methane from the natural gas undergoing partial oxidation producing syngas ($CO + H_2$) flowing up to the top of the reactor in a counter-current with respect to ceria flow. In the oxidation reactor, reduced non-stoichiometric ceria is fed from the top and the exhaust gas from the turbine (CO_2+H_2O) is fed from the bottom which moves up reacting with the metal oxide undergoing splitting reaction producing CO and H_2. The oxidized ceria is transported away from the bottom by a rotating conveyor system (not shown) to the reduction reactor. Since the oxidation reaction is exothermic, there will be a ΔT along the length of the reactor.

Each reactor was modelled as a series of rigorously continuous stirred reactors (RCSTR) interconnected in Aspen Plus. The RCSTR reactor is widely used in the simulation for the multiphase flow having the characteristic of the homogeneous conditions for all phases. The total volume of the reactor is a summation of all the RCSTR reactors connected in series. The reaction kinetics developed by model fitting the experimental data was written in FORTRAN as a user-kinetic subroutine for both reduction and oxidation and hooked to each RCSTR reactor in the moving bed reactor model in Aspen plus shown in Fig. 13. A few specific assumptions were considered for developing the moving bed reactors models. These include assuming all the RCSTRs in reduction reactor to be modelled as isothermal reactors and those for the oxidation reactor to be modelled as adiabatic reactors. The reduction and oxidation kinetic model developed considering all species taking part in reactions are described in the following section. The residence time in each RCSTR was calculated based on the bed volume with respect to ceria in-flow neglecting the volume change due to change in the composition from reactions. Finally, no change in the phase of ceria during redox recycling in the CL unit was considered.

The number of RCSTRs selected for each reactor model relates to accuracy and time for simulation. Considering a methodology for optimizing the number of RCSTRs with respect to accuracy and the convergence time described by Farooqui et al. [20], an iterative procedure was to select the number of RCSTRs for which the relative change in the output of selectivity of CO and H_2 in both the reactors were less than 0.25%. Correspondingly, 8 RCSTRs for the reduction reactor and 10 for oxidation reactor were chosen. However, for higher flexibility of the model, 10 RCSTRs were chosen in series to represent both the RED and OXI reactors.

Please cite this article as: Farooqui A et al., Assessment of integration of methane-reduced ceria chemical looping CO_2/H_2O splitting cycle to an oxy-fired power plant, International Journal of Hydrogen Energy, https://doi.org/10.1016/j.ijhydene.2019.12.182

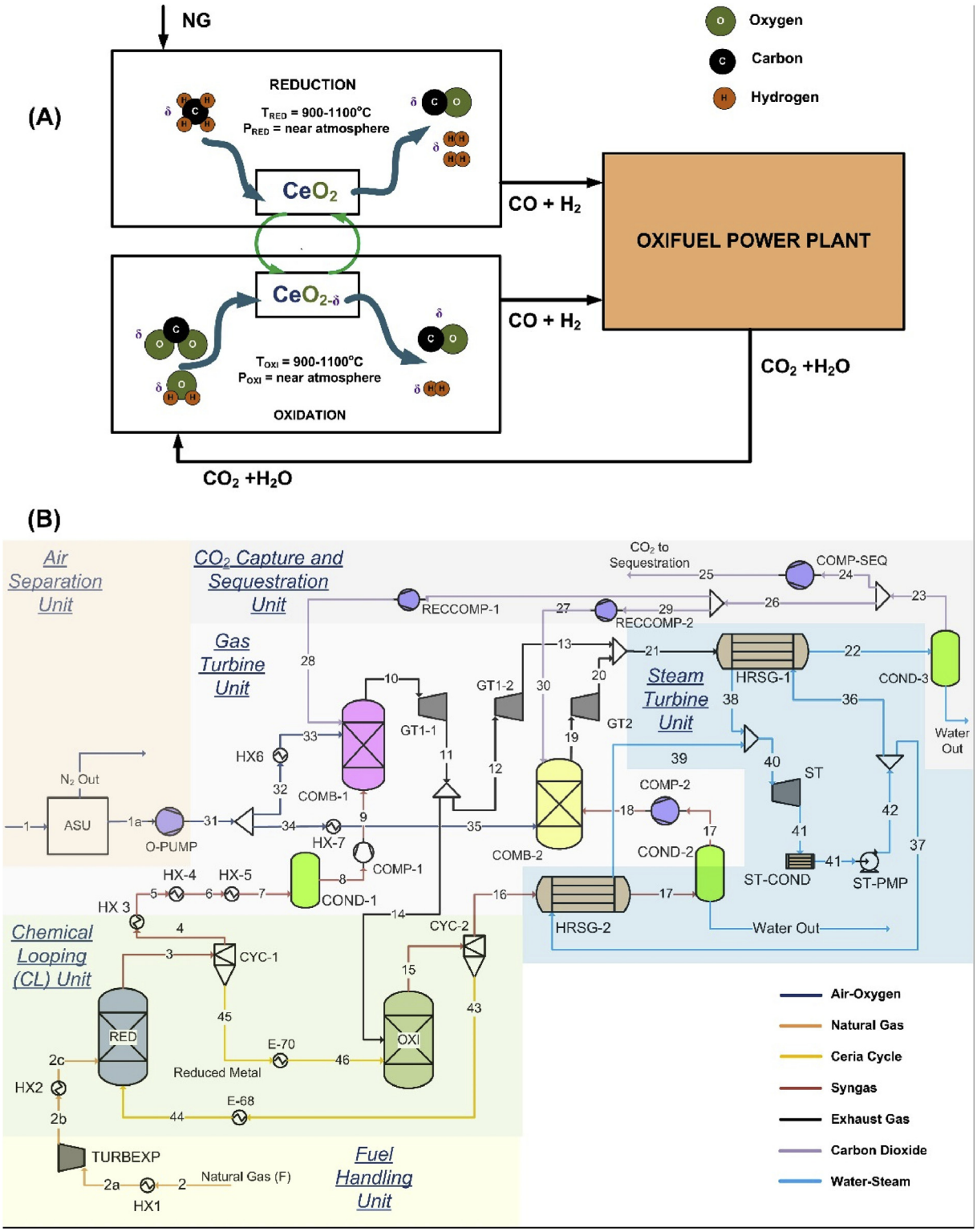

Fig. 12 – (A) Schematic of the chemical looping unit integrated with oxyfuel power plant (B) detailed process layout of oxy-fired power plant OXY-CC-CL [2].

Please cite this article as: Farooqui A et al., Assessment of integration of methane-reduced ceria chemical looping CO_2/H_2O splitting cycle to an oxy-fired power plant, International Journal of Hydrogen Energy, https://doi.org/10.1016/j.ijhydene.2019.12.182

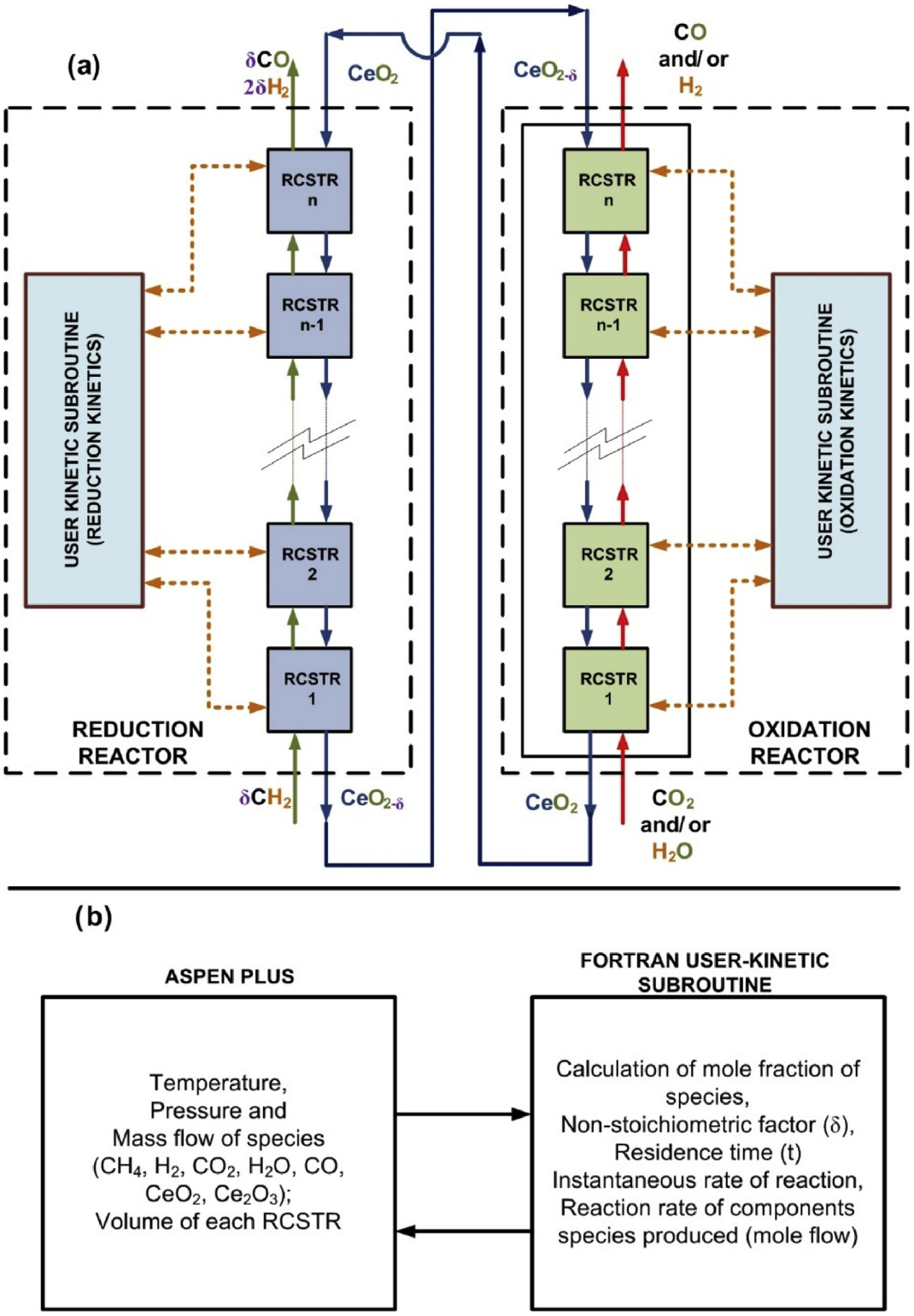

Fig. 13 – Moving bed reactor model for methane reduction and CO_2/H_2O oxidation reactors in ASPEN Plus hooked with user kinetics written in an external FORTRAN Code.

In Aspen plus, Broyden solver was selected with 500 iterations for both mass and energy solvers with a relative tolerance of 0.0001 and the PR-BM method which utilizes the Peng-Robinson cubic equation of state with the Bostone Mathias alpha function [74] is selected for the simulations.

Reduction and oxidation kinetics linked in moving bed reactor model

As previously reported in the introduction of the non-stoichiometric reaction (δ) of ceria during the methane

Please cite this article as: Farooqui A et al., Assessment of integration of methane-reduced ceria chemical looping CO_2/H_2O splitting cycle to an oxy-fired power plant, International Journal of Hydrogen Energy, https://doi.org/10.1016/j.ijhydene.2019.12.182

reduction and oxidation steps can be described by equations (3) and (2). However, due to limited thermodynamic data available in the literature about the non-stoichiometric form of ceria ($CeO_{2-\delta}$), a different approach was adopted using the fully reduced form of ceria Ce_2O_3, which is investigated in the literature [26,38]. Consequently, the equations (3), (2a) and (2b) were rearranged in a different form (21–23) [75]:

$$CeO_2 + \delta CH_4 \rightarrow (1 - 2\cdot\delta)CeO_2 + \delta Ce_2O_3 + 2\cdot\delta H_2 + \delta CO \quad (21)$$

$$(1 - 2\cdot\delta)CeO_2 + \delta Ce_2O_3 + \delta CO_2 \rightarrow CeO_2 + \delta CO \quad (22)$$

$$(1 - 2\delta)CeO_2 + \delta Ce_2O_3 + \delta H_2O \rightarrow CeO_2 + \delta H_2 \quad (23)$$

In this case, the non-stoichiometric factor was used as an indicator of the ratio between the reduced ceria (Ce_2O_3) and the maximum amount of Ce_2O_3 achievable as described in equation (24).

$$\delta = \frac{\dot{n}_{Ce_2O_3}}{2\cdot\dot{n}_{Ce_2O_3} + \dot{n}_{CeO_2}} \quad (24)$$

Therefore, a fully reduced CeO_2 correspond a δ equal to 0.5. However, since the proposed kinetic is based on the non-stoichiometric reduction of ceria, in order to guarantee the stability of the lattice structure of the metal oxide, a limit to the δ equal to 0.35 (δ_{max}) was selected. Henceforth, according to the model proposed by Bulfin et al. [47], the degree of advancement of the reduction reaction, X_{RED}, was calculated as follow:

$$X_{RED} = \frac{\delta}{\delta_{max}} \quad (25)$$

So, the reduction reaction is considered fully completed ($X_{RED} = 1$) when the non-stoichiometric factor reaches the δ_{max}. Conversely, the degree of advancement of the oxidation reactor (X_{OXI}), which occurs in the opposite direction of reduction, was calculated as the complementary of X_{RED}.

$$X_{OXI} = 1 - X_{RED} = 1 - \frac{\delta}{\delta_{max}} \quad (26)$$

Based on the results of the experiments and the kinetic model selected to describe the reduction an oxidation reaction, the reduction reaction rate of ceria that follows the AE3 kinetic model is given as equation (27). In deriving so, equation (12) of solid conversion (X) is used. Non-stoichiometry (δ) is evaluated based on equation (24) and Solid conversion in reduction (X_{RED}) and oxidation (X_{OXI}) reaction is evaluated by equations (25) and (26) which is used in equation (27) for determining reactions rates through kinetic-subroutine in the chemical looping unit explained in Fig. 13.

$$\frac{dX_{RED}}{dx} = A_{RED}\cdot\exp\left(-\frac{E_{RED}}{RT}\right)\cdot 3(1 - X_{RED})[-\ln(1 - X_{RED})]^{2/3}\cdot[CH_4]^{m_{RED}} \quad (27)$$

E_{RED} is the activation energy, A_{RED} is the pre-exponential constant with m_{RED} is the reactor order and their details are presented in section Kinetic study. The changes of molar flow rates of all the species involving in the reduction reaction is represented by equation (28) based on the solid conversion considering reactant flow rates and temperature and molar fractions [20,75,76]. Vector of reduction reaction rates created with this approach is returned to the user-kinetics subroutine and is used to assess change in the components flow. The reduction reaction coefficient (a_{RED}) for the each species taking part in the reaction are listed in Table 1 based on the equation (21).

$$\Delta\dot{n}_{RED-i} = a_{RED-i}\cdot\dot{n}_{CeO_2}\frac{dX_{RED}}{dt}\Delta t \quad (28)$$

$\Delta\dot{n}_{RED\text{-}i}$ is change in component flow rates of species i listed as CeO_2, Ce_2O_3, CH_4, CO, H_2; Δt is the reaction time step which is calculated based on inlet volume flow of the ceria into the differential volume of the reactor and can be represented as equation (29).

$$\Delta t = \frac{\dot{V}_{OC,in}}{\Delta V_{reactor}} \quad (29)$$

Similarly, oxidation kinetics for CO_2 splitting which also follows the nucleation and growth Avrami Erofe'ev AE3 model as evaluated from the experimental analysis presented in section Kinetic study and it can be described by equation (30).

$$\frac{dX_{OXI-CO_2}}{dx} = A_{OXI-CO_2}\cdot\exp\left(-\frac{E_{OXI-CO_2}}{RT}\right)\cdot 3(1 - X_{OXI-CO_2})[-\ln(1 - X_{OXI-CO_2})]^{2/3}\cdot[CO_2]^{m_{OXI}} \quad (30)$$

$A_{OXI\text{-}CO2}$ and $E_{OXI\text{-}CO2}$ are the pre-exponential factor and the activation energy of oxidation reaction step with CO_2 as oxidizer as presented in section Kinetic study.

For H_2O splitting, reaction kinetics model is adopted from Arifin [9] and Arifin and Weimer [44]. The reaction rate for oxidation reaction is represented as equation (31) and coefficients are presented in Table 3.

$$\frac{dX_{OXI-H_2O}}{dt} = A_{OXI-H_2O}\cdot\exp\left(-\frac{E_{OXI-H_2O}}{RT}\right)\cdot[H_2O]_i^{n_o}\cdot(1 - X_{OXI-H_2O})^{\psi_0} \quad (31)$$

$A_{OXI\text{-}H2O}$ is the Arrhenius constant, $E_{OXI\text{-}H2O}$ is the activation energy and n_o is the reaction order for the H_2O splitting

Table 1 – Reduction reaction coefficients.

i	Reduction reaction coefficient (a_{RED})
CeO_2	−2
Ce_2O_3	1
CH_4	1
CO	1
H_2	2

Please cite this article as: Farooqui A et al., Assessment of integration of methane-reduced ceria chemical looping CO_2/H_2O splitting cycle to an oxy-fired power plant, International Journal of Hydrogen Energy, https://doi.org/10.1016/j.ijhydene.2019.12.182

Table 2 – Kinetic parameters of the oxidation reaction of reduced ceria obtained by Arifin [44].

Oxidant	T (°C)	$A_{0,OXI-H2O}$ (1/s)	$E_{0,OXI-H2O}$ (KJ/mol)	ψ_0 (–)	n_o(–)
H_2O	750–800	3.4	45	0.65	1.2
	825–875	2.5	41	0.7	1.7

reaction. These parameters are listed in Table 2. Vectors of oxidation reaction rates created with this approach is returned to the user-kinetics subroutine for each species for the CO_2 and H_2O splitting is represented as equations (32) and (33).

$$\Delta\dot{n}_{OXI-j} = a_{OXI-j}\cdot\dot{n}_{Ce_2O_3}\frac{dX_{OXI-j}}{dt}\Delta t \quad (32)$$

$$\Delta\dot{n}_{OXI-l} = a_{OXI-l}\cdot\dot{n}_{Ce_2O_3}\left\{\frac{dX_{OXI-H_2O}}{dt}+\frac{dX_{OXI-CO_2}}{dt}\right\}\Delta t \quad (33)$$

where $\Delta\dot{n}_{OXI-j}$ change in component flow rates of species listed as H_2O, H_2, CO_2, CO and $\Delta\dot{n}_{OXI-l}$ is for CeO_2,Ce_2O_3 and the reaction coefficient (a_{OXI}) is given in Table 3 based on the equations (22) and (23).

Performance evaluation

To improve on the thermodynamic evaluations reported by Farooqui et al. [2], the RGIBBS reactors for the RED and OXI were replaced by moving bed reactors model, into the described OXY-CC-CL unit and the energetic performance of the proposed plant layout was evaluated. As for the oxidation reaction, since the primary component of the exhaust from the combustor comprises over 86% CO_2, the available water splitting kinetics were used alongside the newly developed CO_2 splitting kinetics by in-house experiments described in the previous section Kinetic study. Based on the experimental results, an isothermal reduction reactor to be operated at 1000 °C was considered in the kinetic-based CL model. To explain the comparative results of the overall plant performance, it is crucial to understand separately the efficiency of the CL unit as a separate entity and the efficiency of the entire layout is crucial. In this regard, the efficiency of the CL unit, was calculated from equation (34).

$$\eta_{SCL}=\frac{\left(\dot{m}_{H_2}LHV_{H_2}+\dot{m}_{CO}LHV_{CO}\right)_{RED}+\left(\dot{m}_{H_2}LHV_{H_2}+\dot{m}_{CO}LHV_{CO}\right)_{OXI}}{\left(\dot{m}_{CH_4}LHV_{CH_4}+\left(\dot{Q}_{RED}-\dot{Q}_{OXI}\right)+\dot{Q}_{NG}\right)+\dot{Q}_{Gas}+\left(\dot{Q}_{sphtr}-\dot{Q}_{sld}\right)} \quad (34)$$

$\dot{Q}_{NG}$ is the heat expended for pre-heating natural gas exiting the turbo-expander to the condition necessary for the RED; $\dot{Q}_{RED}$ is the heat requirement at the reduction reactor. Since for the present configuration, the OXI is an adiabatic reactor, therefore, $\dot{Q}_{OXI}$ is 0. Again, as $\dot{Q}_{Gas}$ accounts for the heat needed to heat the inlet CO_2 and water to the OXI inlet temperature and the exhaust of the turbine is directly sent to the oxidation unit, no heat-up of the same is necessary. $\dot{Q}_{sld}$ represents the heat recovered from the solids from the reduction reactor before it enters oxidation, while $\dot{Q}_{spht}$ is the heat delivered to the solids for preheating. However, being an isothermal system, in a steady state operation, no additional heating or cooling of the solids would be required. Nonetheless, it was ensured that no temperature cross-over takes place.

The results of the comparative evaluation of the performance of the CL unit from the thermodynamic to the kinetic evaluation is shown in Table 4. The thermodynamic evaluation was obtained from the previous study as mentioned above [2]. As can be seen, all other parameters being constant, the net energy rate content in the syngas formation in both the reactors is much less while considering kinetic assessment than the thermodynamic assessment. Indeed, for a lower non-stoichiometry, more specifically, 0.29, obtained in a 10 m^3 reduction reactor, a lower volume of syngas in both the reduction and oxidation reactor (6 m^3) is generated, unlike in thermodynamics, where a complete reduction of CeO_2 to Ce_2O_3 was assumed with an equivalent non-stoichiometry of 0.5. It is to be highlighted that the reactor volume was selected based on the iterative increase in reactor size, whereby a further increase in reactor volume would yield a minimal increase in the yield. Furthermore, considering the configuration of the reduction reactor (RED) to be encapsulated inside the combustion chamber, size would be a crucial constraint to ensure the effective operation of the combined system similar to reported by Farooqui et al. [3]. However, a lower non-stoichiometry also ensures the heating load of the reduction reactor to diminish, as compared to the thermodynamic levels. Considering all factors, the overall efficiency of the CL unit drops from 64.07% for ideal conditions to 42.88% for the evaluated operating conditions using developed reaction kinetic models. Also, it should be noted that the outlet temperature of the oxidized metal from the OXI drops to 1350 °C as opposed to 1380 °C obtained in the thermodynamic evaluation, leading to a loss of 4 MW of heat in the former.

Table 3 – Oxidation reaction rate coefficient for water and carbon dioxide splitting.

j	Reaction coefficient (a_{OXI})	l	Reaction coefficient(a_{OXI})
H_2O	−1	CeO_2	2
H_2	1	Ce_2O_3	−1
CO_2	−1		
CO	1		

Table 4 – Comparison between the layout with thermodynamic (OXY-CC-CL) and kinetic (OXY-CC-CL-K) evaluation of the CL unit.

Parameter	Units	OXY-CC-CL	OXY-CC-CL-K
Heat Rate of Syngas from RED	MW	589.186	375.961
Heat Rate of Syngas from OXI	MW	227.101	134.541
Net Heat Rate of the Syngas Generated (H_2+CO)	MW	816.287	510.502
Q_{RED-IN}	MW	231.433	149.65
$Q_{OXI-OUT}$	MW	−4.44	0
Q_{NG}	MW	57.38	51.19
Heat Rate of the Inlet Fuel (NG)	MW	989.667	989.667
η_{SCL}	–	64.07%	42.88%

Please cite this article as: Farooqui A et al., Assessment of integration of methane-reduced ceria chemical looping CO_2/H_2O splitting cycle to an oxy-fired power plant, International Journal of Hydrogen Energy, https://doi.org/10.1016/j.ijhydene.2019.12.182

Nevertheless, such a high temperature of metal oxide in the RED, even though will considerably decrease the heat requirement of the reaction, might result in carbon deposition to occur as seen through experimental evaluations. Therefore, a detailed design optimization from multiple design perspectives needs to be assessed in further detail, which is beyond the scope of the present study.

Unlike the efficiency of the CL unit, the plant efficiency depends not only on the net syngas generated in the CL unit but also on the total heat balance within the plant. Table 5 lists the comparison of the plant data for the thermodynamic assessment of the CL unit and the kinetic assessment of the same, all other parameters being kept constant. Since the combustion is a highly exothermic spontaneous reaction, no kinetic study assessment of combustion is necessary. And as no other chemical reactions occur in the plant, the kinetic assessment of the CL unit would well describe the performance of the power plant to the more actual extent.

Multiple points of comparison of stream flow rates of same layout considering thermodynamic and kinetic-based chemical looping unit can be observed which is reported in Table S3. The net efficiency of the plant increases slightly from 50.7% for the thermodynamic model to 50.96% utilising a kinetic model of the CL unit. Due to the lower reduction extent in the RED, a lower non-stoichiometry of the reduced ceria is generated, also requiring lower heat for the reaction (by as much as 80 MW than in the thermodynamic assessment). This increases the amount of CO_2 to be recycled to the combustor chamber to maintain the TIT. A 5% excess of exhaust gas from the outlet of the GT at 921 °C was sent to the OXI reactor to ensure complete oxidation of the reduced metal oxide. However, a large excess might decrease the temperature of both the gas and metal oxide at the outlet of the OXI and hence a critical judgment of the same is required. Even though the metal oxide outlet temperature was maintained at a high of 1350 °C, based on the counter-current moving bed configuration of the OXI, the gas outlet temperature from the OXI drops considerably to 1120 °C, as opposed 1380 °C for the thermodynamic layout assessment. This lowers the heat availability within the system. On the contrary, however, the outlet temperature from the RED increases as well from 905 °C to 1000 °C from the thermodynamic to the kinetic model. Besides, the composition of the syngas produced being varying significantly between the two models as shown in Table S4; the heat transfer characteristics are different as well.

Table 5 – Plant Data Comparison of the layout based on thermodynamic (OXY-CC-CL) and kinetic evaluation of the CL unit (OXY-CC-CL-K).

Plant data	Units	OXY-CC-CL	OXY-CC-CL-K
Fuel Energy Input, LHV (A)	MW	990.708	990.708
Net GT Output	MW	484.233	523.488
ST Output	MW	255.937	251.003
Gross Electric Power Output (B)	MW	750.206	774.491
ASU Consumption + O_2 compression	MW	63.383	63.021
CO_2 Capture and Compression	MW	19.222	18.021
Power Cycle Pumps	MW	3.287	3.1
Air/Recycled CO_2 Compression	MW	142.8797	153.61
Syngas Compressors	MW	17.1881	31.833
Total Parasitic Power Consumption (C)	MW	245.959	269.585
Net Electrical Power Output (D = B-C)	MW	504.247	504.906
Gross Electrical Efficiency (B/A*100)	MW	75.72%	78.18%
Net Electrical Efficiency (D/A*100)	%	50.70%	50.96%
CO_2 Capture Efficiency	%	100%	100%
CO_2 captured	t/h	178.658	178.658
Energy Output per tonne of CO_2 Captured	MWh/t	2.822	2.826

With more CO_2 being recycled to the COMB1, and the TIT being constant, the power production in the GT was found to increase during kinetic assessment. However, this was counteracted by the increase in the auxiliary power demand for increased CO_2 recycling for COMB1. As for the secondary cycle from exhaust gas recycling, due to a lower non-stoichiometry generated from reduction, both the energy production in GT2 and auxiliary consumption for the COMB2 decreases, as can be seen from the results in Table 5. Furthermore, a lower temperature of the syngas from the OXI results in a lower steam generation in HRSG-2. Therefore, even though the total gas expanded in GT1 and GT1-2 increases, the gas expanded in GT2 falls. The combined effect leads to a net drop in the power generated in the ST in the kinetic evaluation as compared to the thermodynamic evaluation.

In summary, as can be followed from Table 5, the net efficiency of the power plant is governed by the output from the GT, by far the single largest energy generating unit of the power plant. Even though the auxiliary consumption increases, the net efficiency of the power plant increases slightly for a lower non-stoichiometry resulting from integrating kinetics of methane reduction and corresponding oxidation of the reduced metal oxide by CO_2 and H_2O. Nevertheless, it needs to be highlighted that similar to the thermodynamic system, the kinetic layout is also a non-optimized one. Therefore, to develop a more even comparison between the maximum achievable efficiency by complete heat integration between the two layouts, a pinch analysis for the latter is required is studied. A clear comparison to the pinch analysis of the layout using the thermodynamic assessment and kinetic-based layout, as presented in Fig. 14 can be drawn. Unlike the available 350 MW of high-temperature heat above 200 °C for the thermodynamic layout, the system with the kinetics of the CL unit seems to be completely optimized without any heat available for further improvement of system performance. Therefore, the maximum achievable electrical efficiency is also limited to the present obtained value of 50.96%, as opposed to 61.4% achievable by system optimization of the thermodynamic layout. However, even with kinetic limitations of the reduction and oxidation reactions, an efficiency of 50.96% would ensure a reduction in the energy penalty, from 11.6 to only 3.8 percentage points, a significant benefit of the proposed layout.

In fact, a net economic comparison with the thermodynamic layout was also performed, which are of interest due to the relative change in the sizes of the turbine and the compressors, resulting from a lower non-stoichiometry of ceria reduction. The total TOC of the plant was calculated as $1224 million, around $3 million lower than the corresponding

Please cite this article as: Farooqui A et al., Assessment of integration of methane-reduced ceria chemical looping CO_2/H_2O splitting cycle to an oxy-fired power plant, International Journal of Hydrogen Energy, https://doi.org/10.1016/j.ijhydene.2019.12.182

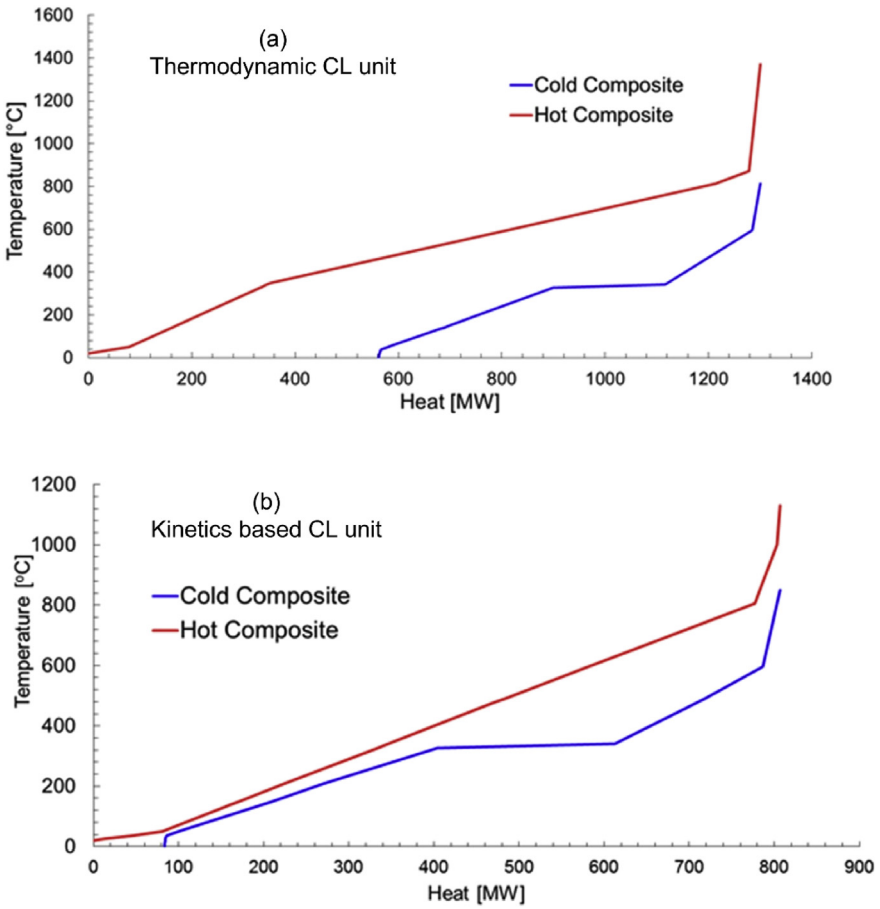

Fig. 14 – Pinch Analysis of the proposed plant based on (a) thermodynamics model of CL unit in OXY-CC-CL unit and (b) kinetics-based moving bed CL unit in layout (OXY-CC-CL-K).

CAPEX calculated using thermodynamic evaluation of the layout. This change is however insignificant with respect to the other operating costs of the power plant as reported by Farooqui et al. [2] and thus not elaborated further.

Conclusions

In the present study, the redox kinetics for commercial ceria considering methane for reduction and CO_2 for oxidation was developed after experiments. The produced CO from both reduction and an oxidation step was evaluated for different temperatures (900–1100 °C) and reactant molar fractions. It is observed that with an increase of temperature the CO production rate increases from 900 to 1050 °C and drops at 1100 °C. Even though at 1050 °C, a higher CO yield was achieved with a larger non-stoichiometry being developed, the sample shows higher aggregates formation and carbon formation making it prone to deactivation. Similarly, for higher methane concentration, there is a drop in CO production rate which is also confirmed by SEM indicating carbon deposition. For oxidation, there is a relative increase in CO production with an increase in temperature but with minimal effect of CO_2 concentration. It is also observed that the reduction and oxidation kinetics paradigm has different reaction rates making methane reduction the rate determining step in the overall redox cycle.

Kinetic model fitting was carried out based on the experimental results to describe the reaction of methane for syngas production with commercial ceria and corresponding oxidation with CO_2 over a temperature range of 900–1100 °C, and different concentration of the reactants. The AE3 model of nucleation and grain growth category was found to fit best to the experimental data for both the reduction and oxidation reactions. A varying reaction order with varying reaction conditions was noticed and a relation was obtained for both the cases. Carbon deposition due to methane splitting would limit the operation of the reduction at temperatures over 1100 °C, even though a very fast reaction would result.

The fitted kinetics were applied to investigate the system performance of a previously proposed novel 500 MW NGCC power plant by the same authors incorporating chemical looping CO_2/H_2O splitting for additional power generation by exhaust gas recycling. A moving bed reactors system is developed with multiple RCSTRs in series in Aspen Plus to mimic the moving bed behaviour of gas and solid in counter-

Please cite this article as: Farooqui A et al., Assessment of integration of methane-reduced ceria chemical looping CO_2/H_2O splitting cycle to an oxy-fired power plant, International Journal of Hydrogen Energy, https://doi.org/10.1016/j.ijhydene.2019.12.182

flow direction. The kinetics were hooked using a user-kinetic subroutine. With kinetics, the maximum non-stoichiometry of ceria achieved was 0.29 and the CL unit efficiency (η_{SCL}) was found to be 42.8% compared to 64% when thermodynamics is considered in the CL unit. A pinch point analysis revealed the tight thermal integration of the system during the kinetic assessment. Hence, the electrical efficiency of the whole plant was limited to 50.96% with kinetics instead of 61.4% when a thermally optimized thermodynamic system is considered. The above analysis is a significant step in integrating CO_2/H_2O splitting to existing oxy-fired natural gas-fired power plants with the possibility of extending it to other fossil fuel power plants.

Nomenclature

Property	Value
$X_{CO,out}$	Mole fraction of CO at the exit of the reactor
$\dot{n}_{ox,out}$	Total molar outflow rate of the gas mixture
P^0	Pressure at standard temperature and pressure (STP)
T^0	Temperature at standard temperature and pressure (STP)
$\dot{V}^0_{OXI,in}$, $\dot{V}^0_{RED,in}$	Total volumetric inflow rate in Oxidation and reduction reactor at standard temperature and pressure (STP)
m_{CeO_2}	Mass of the ceria sample used.
δ_1	Non-stoichiometry reached after reduction step
δ_2	Non-stoichiometry reached after the oxidation of ceria step
δ	Bulk-phase non-stoichiometry change
M_{CeO_2}	Molecular weight of ceria
n_{CeO_2}	Moles of ceria
X	Conversion
E_{RED}, $E_{OXI\text{-}CO2}$, $E_{OXI\text{-}H2O}$	Activation energy of reduction step, CO_2 and H_2O splitting respectively
R	Gas constant that is equal to 8.314 J-mol/K
T	Temperature of the reaction (K)
$A_{OXI\text{-}CO2}$, $A_{OXI\text{-}H2O}$, A_{RED}	Arrhenius exponent for CO2, H2O splitting reaction and Reduction step respectively
K	Reaction rate constant
g(X)	Integral function of f(X)
$\dot{n}_{CO,red}$, $\dot{n}_{CO,oxd}$	Molar flow rates of CO produced during reduction and oxidation
θ	Bragg's angle
β	width at half maximum intensity
λ	Wavelength
D	Grain size
P	Partial pressure
Δt	Reaction time step
$\Delta V_{reactor}$	Differential volume of the reactor
a_{RED}, a_{OXI}	Reduction and oxidation reaction coefficient
A_{OXI}	Oxidation reaction coefficient
Q_{NG}	Heating of natural gas
Q_{RED}	Heat requirement at the reduction reactor
Q_{sld}	Heat recovered from the solids from the reduction reactor
Q_{spht}	Heat delivered to the solids for preheating
m_{RED}, m_{OXI}	Reaction order of reduction step and CO_2 splitting step
n_o	Reaction order of H_2O splitting step
$\Delta\dot{n}_{RED\text{-}i}$	Change in molar flow rates of species $i = CeO_2$, Ce_2O_3, CH_4, CO, H_2
$\Delta\dot{n}_{OXI\text{-}j}$	Change in component flow rates of species listed as H_2O, H_2, CO_2, CO
$\Delta\dot{n}_{OXI\text{-}l}$	Change in component flow rates of species listed as CeO_2,Ce_2O_3
CL	Chemical Looping Unit
CCS	Carbon Capture and Sequestration
CDS	Carbon Dioxide Splitting
WS	Water Splitting
SS	Solid-State
SB	Sestak-Berggren model
RSS	Residual Sum of Squares
AICc	Akaike Information Criterion
OC	Oxygen Carrier
POM	Partial Oxidation of Methane
QMS	Quadrupole Mass Spectrometer
QGA	Quantitative Gas Analyser
XRD	X-ray diffraction
SEM	Scanning Electron Microscope
AE	Avrami-Erofe'ev
RED	Reduction reactor
OXI	Oxidation reactor
RCSTR	Rigorously continuous stirred reactors
PR-BM	Peng Robinson Boston Mathias equation of state
TIT	Turbine Inlet Temperature
GT	Gas Turbine
CAPEX	Capital expenditure
TOC	Total overnight cost
HSRG	Heat recovery steam generator
LHV	Lower heating value

Appendix A. Supplementary data

Supplementary data to this article can be found online at https://doi.org/10.1016/j.ijhydene.2019.12.182.

REFERENCES

[1] Leung DYC, Caramanna G, Maroto-Valer MM. An overview of current status of carbon dioxide capture and storage technologies. Renew Sustain Energy Rev 2014;39:426–43. https://doi.org/10.1016/j.rser.2014.07.093.

[2] Farooqui A, Bose A, Ferrero D, Llorca J, Santarelli M. Techno-economic and exergetic assessment of an oxy-fuel power plant fueled by syngas produced by chemical looping CO2 and H2O dissociation. J CO2 Util 2018;27:500–17. https://doi.org/10.1016/j.jcou.2018.09.001.

[3] Farooqui A, Di F, Bose A, Ferrero D, Llorca J, Santarelli M. Techno-economic and exergy analysis of polygeneration plant for power and DME production with the integration of chemical looping CO2/H2O splitting. Energy Convers Manag 2019;186:200–19. https://doi.org/10.1016/j.enconman.2019.02.043.

[4] Rafiee A, Panahi M, Khalilpour KR. CO2 utilization through integration of post-combustion carbon capture process with Fischer-Tropsch gas-to-liquid (GTL) processes. J CO2 Util 2017;18:98–106. https://doi.org/10.1016/j.jcou.2017.01.016.

Please cite this article as: Farooqui A et al., Assessment of integration of methane-reduced ceria chemical looping CO_2/H_2O splitting cycle to an oxy-fired power plant, International Journal of Hydrogen Energy, https://doi.org/10.1016/j.ijhydene.2019.12.182

[5] Zheng Y, Wei Y, Li K, Zhu X, Wang H, Wang Y. Chemical-looping steam methane reforming over macroporous CeO 2-ZrO2 solid solution: effect of calcination temperature. Int J Hydrogen Energy 2014;39:13361–8. https://doi.org/10.1016/j.ijhydene.2014.04.116.
[6] Zeng D, Qiu Y, Peng S, Chen C, Zeng J, Zhang S, Xiao R. Enhanced hydrogen production performance through controllable redox exsolution within CoFeAlO: X spinel oxygen carrier materials. J Mater Chem A 2018;6:11306–16. https://doi.org/10.1039/c8ta02477d.
[7] Chueh WC, Falter C, Abbott M, Scipio D, Furler P, Haile SM, Steinfeld A. High-Flux solar-driven thermochemical dissociation of CO2 and H2O using nonstoichiometric ceria. Science (80-) 2010;330:1797–801. https://doi.org/10.1126/science.1197834.
[8] Furler P, Scheffe J, Gorbar M, Moes L, Vogt U, Steinfeld A. Solar thermochemical CO2 splitting utilizing a reticulated porous ceria redox system. Energy Fuel 2012;26:7051–9. https://doi.org/10.1021/ef3013757.
[9] Arifin D. Study of redox reactions to split water and carbon dioxide. University of Colorado; 2013. http://scholar.colorado.edu/chbe_gradetds/54.
[10] Scheffe JR, Welte M, Steinfeld A. Thermal reduction of ceria within an aerosol reactor for H_2O and CO_2 splitting. Ind Eng Chem Res 2014;53:2175–82. https://doi.org/10.1021/ie402620k.
[11] Yadav D, Banerjee R. A review of solar thermochemical processes. Renew Sustain Energy Rev 2016;54:497–532. https://doi.org/10.1016/j.rser.2015.10.026.
[12] Zeng L, Cheng Z, Fan JA, Fan LS, Gong J. Metal oxide redox chemistry for chemical looping processes. Nat Rev Chem 2018;2:349–64. https://doi.org/10.1038/s41570-018-0046-2.
[13] Ma S, Chen S, Soomro A, Zhu M, Xiang W. Characterization of FeO 3/CeO2 oxygen carriers for chemical looping hydrogen generation. Int J Hydrogen Energy 2018;43:3154–64. https://doi.org/10.1016/j.ijhydene.2017.12.111.
[14] Wheeler VM, Zapata J, Kreider P, Lipinski W. Effect of non-stoichiometry on optical, radiative, and thermal characteristics of ceria undergoing reduction. Opt Express 2018;26:1238–43. https://doi.org/10.1364/oe-26-10-A360.
[15] Agrafiotis C, Roeb M, Sattler C. A review on solar thermal syngas production via redox pair-based water/carbon dioxide splitting thermochemical cycles. Renew Sustain Energy Rev 2015;42:254–85. https://doi.org/10.1016/j.rser.2014.09.039.
[16] Scheffe JR, Steinfeld A. Thermodynamic analysis of cerium-based oxides for solar thermochemical fuel production. Energy Fuel 2012;26:1928–36. https://doi.org/10.1021/ef201875v.
[17] Riaz A, Ali MU, Lipiński W, Lowe A. Enhanced oxygen exchange capacity in nano-structured vanadia–ceria multi-phase oxygen carriers for solar thermal fuel production. J Mater Chem A 2019;7:27347–60. https://doi.org/10.1039/C9TA06471K.
[18] Brendelberger S, von Storch H, Bulfin B, Sattler C. Vacuum pumping options for application in solar thermochemical redox cycles – assessment of mechanical-, jet- and thermochemical pumping systems. Sol Energy 2017;141:91–102. https://doi.org/10.1016/j.solener.2016.11.023.
[19] Brendelberger S, Vieten J, Roeb M, Sattler C. Thermochemical oxygen pumping for improved hydrogen production in solar redox cycles. Int J Hydrogen Energy 2019;44:9802–10. https://doi.org/10.1016/j.ijhydene.2018.12.135.
[20] Farooqui A, Bose A, Ferrero D, Lorca J, Santarelli M. Simulation of two-step redox recycling of non-stoichiometric ceria with thermochemical dissociation of CO2/H2O in moving bed reactors – Part 1: model development with redox kinetics and sensitivity analysis. Chem Eng Sci 2019. https://doi.org/10.1016/j.ces.2019.03.050.
[21] Otsuka K, Ushiyama T, Yamanaka I. Partial oxidation of methane using the redox of cerium oxide. Chem Lett 1993;22:1517–20. https://doi.org/10.1246/cl.1993.1517.
[22] Pantu P, Kim K, Gavalas GR. Methane partial oxidation on Pt/CeO2–ZrO2 in the absence of gaseous oxygen. Appl Catal A Gen 2000;193:203–14. https://doi.org/10.1016/S0926-860X(99)00429-9.
[23] Nair MM. Tailoring hybrid nonstoichiometric ceria redox cycle for combined solar methane reforming and thermochemical conversion of H 2 O/. 2016. https://doi.org/10.1021/acs.energyfuels.6b01063.
[24] Krenzke PT, Fosheim JR, Zheng J, Davidson JH. Synthesis gas production via the solar partial oxidation of methane-ceria redox cycle: conversion, selectivity, and efficiency. Int J Hydrogen Energy 2016;41:12799–811. https://doi.org/10.1016/j.ijhydene.2016.06.095.
[25] Welte M, Warren K, Scheffe JR, Steinfeld A. Combined ceria reduction and methane reforming in a solar-driven particle-transport reactor. Ind Eng Chem Res 2017;56:10300–8. https://doi.org/10.1021/acs.iecr.7b02738.
[26] Nair MM, Abanades S. Tailoring hybrid nonstoichiometric ceria redox cycle for combined solar methane reforming and thermochemical conversion of H2O/CO2. Energy Fuel 2016;30:6050–8. https://doi.org/10.1021/acs.energyfuels.6b01063.
[27] Krenzke PT, Fosheim JR, Davidson JH. Solar fuels via chemical-looping reforming. Sol Energy 2017;156:48–72. https://doi.org/10.1016/j.solener.2017.05.095.
[28] Kodama T, Gokon N. Thermochemical cycles for high-temperature solar hydrogen production. Chem Rev 2007;107:4048–77. https://doi.org/10.1021/cr050188a.
[29] Lorentzou S, Dimitrakis D, Zygogianni A, Karagiannakis G, Konstandopoulos AG. Thermochemical H2O and CO2splitting redox cycles in a NiFe2O4structured redox reactor: design, development and experiments in a high flux solar simulator. Sol Energy 2017;155:1462–81. https://doi.org/10.1016/j.solener.2017.07.001.
[30] Lapp J. Thermal modeling and design of a solar non-stoichiometric redox reactor with heat recovery. 2013. http://conservancy.umn.edu/handle/11299/159856.
[31] Roeb M, Sattler C, Klüser R, Monnerie N, de Oliveira L, Konstandopoulos AG, Agrafiotis C, Zaspalis VT, Nalbandian L, Steele A, Stobbe P. Solar hydrogen production by a two-step cycle based on mixed iron oxides. J Sol Energy Eng 2006;128:125. https://doi.org/10.1115/1.2183804.
[32] Davenport TC, Yang CK, Kucharczyk CJ, Ignatowich MJ, Haile SM. Maximizing fuel production rates in isothermal solar thermochemical fuel production. Appl Energy 2016;183:1098–111. https://doi.org/10.1016/j.apenergy.2016.09.012.
[33] Otsuka K, Wang Y, Sunada E, Yamanaka I. Direct partial oxidation of methane to synthesis gas by cerium oxide. J Catal 1998;175:152–60. https://doi.org/10.1006/jcat.1998.1985.
[34] Lin F, Rothensteiner M, Alxneit I, van Bokhoven JA, Wokaun A. First demonstration of direct hydrocarbon fuel production from water and carbon dioxide by solar-driven thermochemical cycles using rhodium-ceria. Energy Environ Sci 2016. https://doi.org/10.1039/C6EE00862C.
[35] Lin F, Wokaun A, Alxneit I. Rh-doped ceria: solar organics from H2O, CO2 and sunlight? Energy Procedia 2015. https://doi.org/10.1016/j.egypro.2015.03.151.
[36] Warren KJ, Reim J, Randhir K, Greek B, Carrillo R, Hahn DW, Scheffe JR. Theoretical and experimental investigation of solar methane reforming through the nonstoichiometric ceria redox cycle. Energy Technol 2017;5:2138–49. https://doi.org/10.1002/ente.201700083.

Please cite this article as: Farooqui A et al., Assessment of integration of methane-reduced ceria chemical looping CO_2/H_2O splitting cycle to an oxy-fired power plant, International Journal of Hydrogen Energy, https://doi.org/10.1016/j.ijhydene.2019.12.182

[37] Otsuka K, Sunada E, Ushiyama T, Yamanaka I. The production of synthesis gas by the redox of cerium oxide. Stud Surf Sci Catal 1997;107:531–6. https://doi.org/10.1016/S0167-2991(97) 80386-2.
[38] Warren KJ, Scheffe JR. Kinetic insights into the reduction of ceria facilitated via the partial oxidation of methane. Mater Today Energy 2018;9:39–48. https://doi.org/10.1016/j.mtener.2018.05.001.
[39] Chueh WC, Haile SM. A thermochemical study of ceria: exploiting an old material for new modes of energy conversion and CO2 mitigation. Philos Trans R Soc A Math Phys Eng Sci 2010;368:3269–94. https://doi.org/10.1098/rsta.2010.0114.
[40] Le Gal A, Abanades S. Catalytic investigation of ceria-zirconia solid solutions for solar hydrogen production. Int J Hydrogen Energy 2011;36:4739–48. https://doi.org/10.1016/j.ijhydene.2011.01.078.
[41] Le Gal A, Abanades S, Flamant G. CO2 and H2O splitting for thermochemical production of solar fuels using nonstoichiometric ceria and ceria/zirconia solid solutions. Energy Fuel 2011;25:4836–45. https://doi.org/10.1021/ef200972r.
[42] Gotor FJ, José, Criado M, Malek J, Koga N. Kinetic analysis of solid-state reactions: the universality of master plots for analyzing isothermal and nonisothermal experiments. J Phys Chem A 2000;104:10777–82. https://doi.org/10.1021/jp0022205.
[43] Khawam A, Flanagan DR. Solid-state kinetic models: basics and mathematical fundamentals. J Phys Chem B 2006;110:17315–28. https://doi.org/10.1021/jp062746a.
[44] Arifin D, Weimer AW. Kinetics and mechanism of solar-thermochemical H2and CO production by oxidation of reduced CeO2. Sol Energy 2018;160:178–85. https://doi.org/10.1016/j.solener.2017.11.075.
[45] Farooqui AE, Pica AM, Marocco P, Ferrero D, Lanzini A, Fiorilli S, Llorca J, Santarelli M. Assessment of kinetic model for ceria oxidation for chemical-looping CO2 dissociation. Chem Eng J 2018;346:171–81. https://doi.org/10.1016/j.cej.2018.04.041.
[46] Scheffe JR, McDaniel AH, Allendorf MD, Weimer AW. Kinetics and mechanism of solar-thermochemical H2 production by oxidation of a cobalt ferrite–zirconia composite. Energy Environ Sci 2013;6:963. https://doi.org/10.1039/c3ee23568h.
[47] Bulfin B, Lowe AJ, Keogh KA, Murphy BE, Lübben O, Krasnikov SA, Shvets IV. Analytical model of CeO 2 oxidation and reduction. J Phys Chem C 2013;117:24129–37. https://doi.org/10.1021/jp406578z.
[48] Pullar RC, Novais RM, Caetano APF, Barreiros MA, Abanades S, Oliveira FAC. A review of solar thermochemical CO2 splitting using ceria-based ceramics with designed morphologies and microstructures. Front Chem 2019;7. https://doi.org/10.3389/fchem.2019.00601.
[49] Bose A, Farooqui A, Ferrero D, Santarelli M, Llorca J. Thermodynamic assessment of non - catalytic Ceria for syngas production by methane reduction and - CO 2 + H 2 O oxidation. Mater Renew Sustain Energy 2019;3. https://doi.org/10.1007/s40243-019-0142-3.
[50] Kim J, Johnson TA, Miller JE, Stechel EB, Maravelias CT. Fuel production from CO2 using solar-thermal energy: system level analysis. Energy Environ Sci 2012;5:8417. https://doi.org/10.1039/c2ee21798h.
[51] Kim J, Henao CA, Johnson TA, Dedrick DE, Miller JE, Stechel EB, Maravelias CT. Methanol production from CO2 using solar-thermal energy: process development and techno-economic analysis. Energy Environ Sci 2011;4:3122. https://doi.org/10.1039/c1ee01311d.
[52] Falter C, Batteiger V, Sizmann A. Climate impact and economic feasibility of solar thermochemical jet fuel production. Environ Sci Technol 2016;50:470–7. https://doi.org/10.1021/acs.est.5b03515.
[53] Falter C, Pitz-Paal R. Energy analysis of solar thermochemical fuel production pathway with a focus on waste heat recuperation and vacuum generation. Sol Energy 2018;176:230–40. https://doi.org/10.1016/J.SOLENER.2018.10.042.
[54] Abanades A, Ruiz E, Ferruelo EM, Hernandez F, Cabanillas A, Rubio JA, Lopez C, Gavela R, Barrera G, Rubbia C, Salmieri D, Rodilla E, Gutierrez D. Experimental analysis of direct thermal methane cracking. Int J Hydrogen Energy 2011;36:12886. https://doi.org/10.1016/j.ijhydene.2011.07.081.
[55] Guizani C, Javier F, Sanz E, Salvador S. The nature of the deposited carbon at methane cracking over a nickel loaded wood-char la suite de la r La nature du carbone d epos e a eaction de craquage du m ethane sur un char de biomasse charg e en nickel. Compt Rendus Chem 2016;19:423–32. https://doi.org/10.1016/j.crci.2015.10.009.
[56] Fosheim JR, Hathaway BJ, Davidson JH. High efficiency solar chemical-looping methane reforming with ceria in a fixed-bed reactor. Energy 2018. https://doi.org/10.1016/j.energy.2018.12.037.
[57] Lahijani P, Alimuddin Z, Mohammadi M, Rahman A. Conversion of the greenhouse gas CO 2 to the fuel gas CO via the Boudouard reaction : a review. Renew Sustain Energy Rev 2015;41:615–32. https://doi.org/10.1016/j.rser.2014.08.034.
[58] Zhu L, Lu Y. Reactivity and efficiency of ceria-based oxides for solar CO2 splitting via isothermal and near-isothermal cycles. Energy Fuel 2017. https://doi.org/10.1021/acs.energyfuels.7b03284. acs.energyfuels.7b03284.
[59] Muhich C, Steinfeld A. Principles of doping ceria for the solar thermochemical redox splitting of H_2O and CO_2. J Mater Chem A 2017;5:15578–90. https://doi.org/10.1039/C7TA04000H.
[60] Ackermann S, Sauvin L, Castiglioni R, Rupp JLM, Scheffe JR, Steinfeld A. Kinetics of CO2 reduction over nonstoichiometric ceria. J Phys Chem C 2015;119:16452–61. https://doi.org/10.1021/acs.jpcc.5b03464.
[61] Venstrom LJ, De Smith RM, Hao Y, Haile SM, Davidson JH. Efficient splitting of CO 2 in an isothermal redox cycle based on ceria. Energy Fuel 2014;28:2732–42. https://doi.org/10.1021/ef402492e.
[62] Zhao Z, Uddi M, Tsvetkov N, Yildiz B, Ghoniem AF. Redox kinetics study of fuel reduced ceria for chemical-looping water splitting. J Phys Chem C 2016;120:16271–89. https://doi.org/10.1021/acs.jpcc.6b01847.
[63] Rudisill SG, Venstrom LJ, Petkovich ND, Quan T, Hein N, Boman DB, Davidson JH, Stein A. Enhanced oxidation kinetics in thermochemical cycling of CeO 2 through templated porosity. J Phys Chem C 2013;117:1692–700. https://doi.org/10.1021/jp309247c.
[64] Chuayboon S, Abanades S, Rodat S. Syngas production via solar-driven chemical looping methane reforming from redox cycling of ceria porous foam in a volumetric solar reactor. Chem Eng J 2018. https://doi.org/10.1016/j.cej.2018.09.072.
[65] Zhao Z. Redox kinetics study for chemical looping combustion, water and CO2 splitting using nickel and cerium based oxygen carrier. PhD thesis. Massachusetts Institute of Technology; 2016.
[66] Ron J, Robert S. Introduction to X-ray powder diffractometry, vol. 138. John Wiley & Sons, Ltd; 1996. https://doi.org/10.1002/9781118520994.
[67] Steinfeld A, Frei A, Kuhn P, Wuillemin D. Solar thermal production of zinc and syngas via combined ZnO-reduction and CH4-reforming processes. Int J Hydrogen Energy 1995;20:793–804. https://doi.org/10.1016/0360-3199(95)00016-7.

Please cite this article as: Farooqui A et al., Assessment of integration of methane-reduced ceria chemical looping CO_2/H_2O splitting cycle to an oxy-fired power plant, International Journal of Hydrogen Energy, https://doi.org/10.1016/j.ijhydene.2019.12.182

[68] Zhu X, Wang H, Wei Y, Li K, Cheng X. Hydrogen and syngas production from two-step steam reforming of methane using CeO2as oxygen carrier. J Nat Gas Chem 2011;20:281–6. https://doi.org/10.1016/S1003-9953(10)60185-5.
[69] Janković B, Adnađević B, Mentus S. The kinetic study of temperature-programmed reduction of nickel oxide in hydrogen atmosphere. Chem Eng Sci 2008;63:567–75. https://doi.org/10.1016/j.ces.2007.09.043.
[70] Zhao Z, Uddi M, Tsvetkov N, Yildiz B, Ghoniem AF. Enhanced intermediate-temperature CO 2 splitting using nonstoichiometric ceria and ceria–zirconia. Phys Chem Chem Phys 2017;19:25774–85. https://doi.org/10.1039/C7CP04789D.
[71] Galwey AK, Brown ME. Kinetic background to thermal analysis and calorimetry. In: Handb. Therm. Anal. Calorim. vol. 1; 1998. p. 147–216. Princ. Pract.
[72] Ackermann S, Scheffe JR, Steinfeld A. Diffusion of oxygen in ceria at elevated temperatures and its application to H2O/CO2 splitting thermochemical redox cycles. J Phys Chem C 2014;118:5216–25. https://doi.org/10.1021/jp500755t.
[73] Khan MN, Shamim T. Influence of specularity coefficient on the hydrodynamics and bubble statistics of an annular fluidized bed reactor. Energy Procedia 2017;105:1998–2003. https://doi.org/10.1016/j.egypro.2017.03.573.
[74] Fan J, Zhu L, Jiang P, Li L, Liu H. Comparative exergy analysis of chemical looping combustion thermally coupled and conventional steam methane reforming for hydrogen production. J Clean Prod 2016;131:247–58. https://doi.org/10.1016/j.jclepro.2016.05.040.
[75] Farooqui A, Jaroszuk W, Ferrero D, Santarelli M, Llorca J. System efficiency analysis of dual interconnected bubbling fluidized bed reactors for solar fuel production. In: Proc. Int. Conf. ECOS-2018, 31st Int. Effic. Cost, Optim. Simul. Environ. Impact Syst. June 17–22, 2018, Guimares, Port; 2018.
[76] Farooqui A, Bose A, Ferrero D, Lorca J, Santarelli M. Simulation of two-step redox recycling of non-stoichiometric ceria with thermochemical dissociation of CO2/H2O in moving bed reactors – Part II: techno-economic analysis and integration with 100 MW oxyfuel power plant with carbon capture. Chem Eng Sci 2019;205:358–73.

Please cite this article as: Farooqui A et al., Assessment of integration of methane-reduced ceria chemical looping CO_2/H_2O splitting cycle to an oxy-fired power plant, International Journal of Hydrogen Energy, https://doi.org/10.1016/j.ijhydene.2019.12.182